

UC Berkeley

UC Berkeley Electronic Theses and Dissertations

Title

Retinal Image-Based Eye-Tracking Using the Tracking Scanning Laser Ophthalmoscope

Permalink

<https://escholarship.org/uc/item/85b2f4rk>

Author

Sheehy, Christy Kathleen

Publication Date

2015

Supplemental Material

<https://escholarship.org/uc/item/85b2f4rk#supplemental>

Peer reviewed|Thesis/dissertation

Retinal Image-Based Eye-Tracking Using the Tracking
Scanning Laser Ophthalmoscope

By

Christy Kathleen Sheehy

A dissertation submitted in partial satisfaction of the

requirements for the degree of

Doctor of Philosophy

in

Vision Science

in the

Graduate Division

of the

University of California, Berkeley

Committee in charge:

Professor Austin Roorda, Chair

Professor Susana Chung

Professor Laura Waller

Fall 2015

Abstract

Retinal Image-Based Eye-Tracking Using the Tracking Scanning Laser Ophthalmoscope

by

Christy Kathleen Sheehy

Doctor of Philosophy in Vision Science

University of California, Berkeley

Professor Austin Roorda, Chair

The tracking scanning laser ophthalmoscope (TSLO) was designed, built and characterized for high-resolution eye-tracking, imaging, and targeted retinal stimulus delivery. Eye-tracking is done via an image-based software program that monitors the image of the retina over time while simultaneously logging the displacements of the eye. Currently, this system is the most accurate, fast and functional eye-tracking system used in a standard ophthalmic instrument. The TSLO has the ability to non-invasively track the eye at 960 Hz (with an accuracy of 0.2 arcminutes or roughly 1 micron) and present stimuli to the retina at the resolution of single cone photoreceptors (0.66 arcminutes, which is roughly 3 microns). The combination of structural imaging and functional testing allows one to begin to more thoroughly understand retinal disease progression, as well probe specific retinal locations in order to test new treatment efficacies. This level of accuracy is unprecedented in the clinic and is crucial when monitoring minute changes in eye motion, structure, and function. Additionally, the system is capable of providing external eye-tracking for other high-resolution imaging systems, such as optical coherence tomography (OCT) and adaptive optics scanning laser ophthalmoscope (AOSLO) systems through the active steering of an imaging beam. This feature allows the imaging raster or stimuli to stay on target during fixational eye motion. This dissertation steps through all of the above-mentioned uses of the TSLO and further elaborates on the optimal design and system test performance capabilities of the system.

Contents

Abstract.....	1
LIST OF FIGURES.....	iii
LIST OF ABBREVIATIONS	iv
ACKNOWLEDGEMENTS.....	vi
CHAPTER 1: The Tracking Scanning Laser Ophthalmoscope	1
1.1 Introduction.....	1
1.1.1 Fixational Eye Motion.....	1
1.1.2 Current Eye-tracking Technologies and Methods: An Overview	4
Chapter 2: Optical Design and Modelling of the Tracking Scanning Laser Ophthalmoscope	9
2.1 Abstract	9
2.2 Introduction.....	9
2.3 Methods	9
2.3.1 Optical Design and Optimization of the Tracking Scanning Laser Ophthalmoscope	9
2.3.2 Opto-mechanical Design Considerations	13
2.4 Results	14
2.5 Discussion	15
2.6 Summary	16
2.7 Acknowledgements.....	16
CHAPTER 3: Real-time Eye-tracking with the TSLO	17
3.1 Abstract	17
3.2 Introduction.....	17
3.3 Methods	17
3.3.1 Overview of Eye-tracking Software	17
3.3.4 System Resolution	21
3.5 Discussion	21
3.6 Summary	22
3.7 Acknowledgements.....	22
CHAPTER 4: Microperimetry Using the TSLO System	23
4.1 Abstract	23
4.2 Introduction.....	23
4.3 Methods	24

4.3.1 System Design Modifications	24
4.3.2 Stimulus Delivery Accuracy.....	25
4.4 Results	28
4.4.1 Patient 1 (P1) Imaging with Functional Testing.....	29
4.4.2 Patient 2 (P2) Imaging with Functional Testing.....	31
4.5 Discussion	33
4.6 Summary	35
4.7 Acknowledgements.....	35
CHAPTER 5: The Usage of the TSLO as an External Eye-tracker	35
5.1 Abstract	35
5.2 Introduction.....	35
5.3 Methods	37
5.3.1 Optical Design of an AOSLO System for External Eye-tracking	37
5.3.2 Combination of TSLO and AOSLO Systems.....	38
5.3.3 Software and Hardware for Open-loop Tracking	40
5.4 Results	42
5.4.1 System Bandwidth Analysis for active-tracking with a PI mirror	42
5.4.2 Human Eye Motion Frequency Analysis.....	43
5.5 Discussion	47
5.6 Combination of the TSLO with OCT Systems	49
5.6.1 Combination of the TSLO with OFDI OCT System	49
5.7 Summary	54
5.8 Conclusion	54
5.9 Acknowledgements.....	55
Dissertation Summary.....	56
REFERENCES	57

LIST OF FIGURES

Chapter 1:

Figure 1.1: Fixational eye motion mock-up on a photoreceptor cone mosaic.	2
Figure 1.2: Fixational eye motion as a function of frequency	3
Figure 1.3: EyeLink II pupil eye-tracking system.....	7
Figure 1.4: Purkinje reflexes	7

Chapter 2:

Figure 2.1: Front end ZEMAX design of the TSLO system.....	11
Figure 2.2: Geometric spot diagrams.	12
Figure 2.3: Image of the beam as viewed from pupil plane of the eye.....	13
Figure 2.4: Optomechanical design of the TSLO system as modelled in Solidworks.	14
Figure 2.5: A 2-D optical design schematic of the TSLO..	15

Chapter 3:

Figure 3.1: Recovery of eye motion	18
Figure 3.2: Motion amplitude reduction	19
Figure 3.3: Amplitude of eye motion vs. input frequency.....	20
Figure 3.4: Image of the cone photoreceptor mosaic	21

Chapter 4:

Figure 4.1: Opto-mechanical design	25
Figure 4.2: Timelines for targeted stimulus delivery	26
Figure 4.3: Registered AOSLO image	27
Figure 4.4: Stimulus accuracy	28
Figure 4.5: Retinal montage of the subclinical lesion for P1	30
Figure 4.6: Threshold intensity values for P1	31
Figure 4.7: TSLO image with the corresponding OCT scan for P1.....	32
Figure 4.8: Locations of functional testing for P2.....	32

Chapter 5

Figure 5.1: Zemax design of active eye-tracking AOSLO system.	45
Figure 5.2: A 2-D Optical design schematic of the TSLO-AOSLO combination system.....	47
Figure 5.3: Model eye equipped with a galvanometric scanner.	42
Figure 5.4: Amplitude Reduction (%) vs frequency.	50
Figure 5.5: TSLO and AOSLO retinal images.	52
Figure 5.6: Averaged AOSLO video.	53
Figure 5.7: Measured horizontal eye motion traces.	54
Figure 5.8: Measured vertical eye motion traces.....	56
Figure 5.10: The reduction of vertical eye motion as a function of frequency.	56

Figure 5.11: The optical layout of the combined OFDI-TSLO setup	50
Figure 5.12: En face images from 4 different volume data sets.....	52
Figure 5.13: Tracked en face images with validity signal	53
Figure 5.14: High-quality artifact-free angiograms of the retina.	54

LIST OF ABBREVIATIONS

ANSI: American National Standard Institute
 AMD: Age-related macular degeneration
 AO: Adaptive optics
 AOM: Acousto-optic modulator
 AOMP: Adaptive optics microperimetry
 AOSLO: Adaptive optics scanning laser ophthalmoscope (or ophthalmoscopy)
 a.u.: Arbitrary Units
 CM: Curved mirror
 DAC: Digital-to-analog converter
 DC: Direct Current
 dB: Decibels
 DM: Dichroic Mirror
 dPi: Dual-Purkinje
 F = Focal Length
 FFT: Fast Fourier transform
 FOV: Field of view
 FPGA: Field programmable gate array
 FT: Fourier transform
 GCL: Ganglion cell layer
 GPU: Graphics processing unit
 GUI: Graphical user interface
 Hz: Hertz
 I: Intensity
 INL: Inner nuclear layer
 IPL: Inner plexiform layer
 IR: Infrared
 kHz: kilohertz
 L-/M-/S- L-, M-, and S-cones, respectively
 LCA: Longitudinal chromatic aberration
 LSO: Line scanning ophthalmoscopy (or ophthalmoscope)
 M: Magnification
 mfERG: Multi-focal electroretinogram
 mm: Millimeter
 MP1: Nidek microperimeter

ms: Millisecond
NFL: Nerve fiber layer
nm: Nanometer
OCT: Optical coherence tomographer (or tomography)
OFDI: Optical frequency domain imaging
P_{1,2,3,4}: 1st, 2nd, 3rd, and 4th Purkinje images
P1: Patient 1
P2: Patient 2
PC: Personal computer
PI: Physik Instrumente
PMT: Photomultiplier tube
PRL: Preferred retinal locus of fixation
PSF: Point spread function
ROI: Region of interest
S: Scanner
SD: Standard deviation
μm: microns

ACKNOWLEDGEMENTS

*"I've heard it said, that people come into our lives for a reason, bringing something we must learn. And we are led to those who help us most to grow if we let them, and we help them in return." – **Wicked the Musical***

As I sit here at my desk in the Roorda laboratory, just days before I hand in my thesis, I realize how many people I have to thank for this wonderful opportunity to learn and grow. I would like to first thank my family for instilling in me a love of education and a desire to continue learning something new every day. To my mother, in particular, for encouraging me to follow my PhD dreams across the country in sunny California. To my father, for showing me that no matter how tough things may be, laughter is always the best medicine. And to my sister and nephew, Colleen and Nicolas, for showing me that perseverance, and the love and support of family, can always help you attain your goals.

I would also like to thank my colleagues and mentors at the University of Rochester. As an undergraduate student, I had the privilege of working with Dr. David Williams. This opportunity opened my eyes to world of vision research and sparked my passion for retinal imaging. In particular I'd like to thank David Williams, for giving me the opportunity to join his lab, Jessica Morgan, for teaching me how to process and analyze RPE mosaics, Mina Chung, for hiring me as a part-time master's student to analyze photoreceptor mosaics, and Alfredo Dubra for guiding a portion of my master's research project. Additionally, Jennifer Hunter, Ben Masella, Melissa Geng, Jennifer Sentiff, Yusufu Sulai, and my officemate, Robin Sharma, were a constant stream of great ideas and support. For that, I am forever grateful.

To my lab mates at the University of California, Berkeley– you constantly amaze me with your love of science and willingness to help one another. Working with you over the last five and a half years has truly been a gift. To Kavitha Ratnam, for being the best lab mate, friend and cooking buddy a girl could ask for. To Ally Boehm, for being the best TSLO research sidekick extraordinaire (through good times and bad!) and fellow Grand Canyon adventurer. To Natalie Stepien, for being my paddle boarding partner and constant ray of sunshine. To Ethan Bensinger, for being a wonderful lab mate and best friend - you make me so very happy every day, thank you for all you do. To my upper classman lab mates: William Tuten, Ram Sabesan, Bhavna Antony, Nicole Putnam, Johnny Tam, Adam Hickenbotham, Brandon Lujan and Wolf Harmening – I appreciate all the guidance, help, and encouragement you gave me over the last five years. To Wolf especially, thank you for giving me the opportunity to work with you and your lab in Germany for a summer - that experience taught me how to be the best engineer I can be. A special thank you goes to our lab programmer, Pavan Tiruveedhula - my PhD wouldn't have been possible without your constant support and guidance - you are so very much appreciated. To my thesis committee members, Susana Chung and Laura Waller, thank you for your helpful edits and guidance throughout this entire thesis writing process (especially last minute edits!). Lastly, but most importantly, I'd like to thank my mentor, Austin Roorda. Your passion for research and love of the retina has been absolutely inspiring. I feel so very lucky to have been able to work with you and be a part of your lab. Your mentorship and guidance have shaped me into the scientist, engineer, and entrepreneur I am today. Words can't express how appreciative I am of all your support – THANK YOU for letting me into the Roorda Lab family.

CHAPTER 1: The Tracking Scanning Laser Ophthalmoscope

1.1 Introduction

1.1.1 Fixational Eye Motion

The human eye is constantly in motion. Even when fixating on a target, the eye is drifting over dozens to hundreds of photoreceptors sampling the outside world. This constant involuntary movement, known as fixational eye motion, is necessary to prevent an image from perceptually fading away from view. It has been shown to take roughly 80 ms for the perception of a stabilized image to fade away on the retina (Coppola et al., 1996). The principle of stable features fading away is demonstrated in everyday life, as blood vessels are stationary with respect to the retina, causing the meshwork of vasculature to fade away from view. Therefore, constant motion of the eye is necessary to capture the scene.

Fixational eye motion is comprised of involuntary low frequency, low velocity motion called drift and high frequency, jerk-like motions known as microsaccades. Fixational eye motion was first noted by Jurin in 1738 when comparing the visual angle needed to differentiate two marks from one. He reported that a subject needed a larger visual angle to distinguish two marks from a single mark. He hypothesized that this could be due the “trembling” of the eye (Jurin, 1738). Over a century later during the 1860s, Helmholtz postulated that the “wandering of gaze” was present in the eye in order to prevent the development of retinal fatigue (Helmholtz, 1924-1925). This area of interest was further explored as a topic of modern day research in the 1950s by Ratcliff and Riggs. The pair used the optical lever method, securing a mirror to a contact lens, to directly observe fixational eye motion on photographic film (Ratcliff & Riggs, 1950). They observed what they considered to be four types of fixational motion: (1) small rapid motions, (2) relatively slow motion, (3) slow drifts, and (4) rapid jerks (Ratcliff & Riggs, 1950). In more recent literature, these four types of motion have been condensed down to just three main types of fixations. The small rapid motions are commonly referred to as “tremor.” Tremor is the high frequency component of motion, superimposed upon drift, and ranges from 30-80 Hz. Recently, the presence of tremor has been debated, as the typical peak seen near 80-90 Hz using pupil and corneal tracking is not seen using SLOs to record motion (Stevenson et al., 2010). The relatively slow motion and slow drifts have been combined to be just “drift” and the rapid jerks are categorized as “microsaccades.” Figure 1.1 shows an example of how the three different types of fixational eye movements could traverse along the retina. Each individual circular shape represents an individual cone photoreceptor cell.

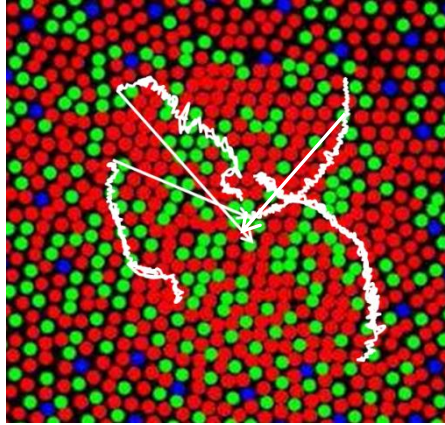


Figure 1.1: Fixational eye motion mock-up on a photoreceptor cone mosaic. Tremor is superimposed onto the slow drift as the high frequency noise component seen above, while microsaccade paths are depicted with the straight-line arrows.

The purpose or function of fixational eye motion has long been studied and debated. It was originally speculated that microsaccades were mainly responsible for returning the drifting point of fixation back to the center of gaze, or the fovea (Cornsweet, 1958). This is the location of the retina with the highest density of cone photoreceptors. However, it was later reported that drifts and microsaccades are both error correcting and error producing (Nachmias, 1961; Steinman, Haddad, Skavenski, and Wyman, 1973), which fueled further research. Due to the fact that microsaccades were shown to be suppressed during high acuity tasks in early literature (Kowler and Steinman, 1979; Winterson and Collewijn, 1976), researchers began to wonder what if any visual purpose they served. In fact, with journal articles entitled “Miniature saccades: eye movements that do not count” (Kowler and Steinman, 1979) and “Small saccades serve no useful purpose” (Kowler and Steinman, 1980), fixational eye motion was not explored again until the late 1990’s. Recent studies have begun to tackle this mystery, providing better insight into its function and purpose. In 2007, Rucci et al. found that fixational motion acts as a filter to enhance the visibility of high spatial frequency information (Rucci et al., 2007). Additionally, microsaccades have been shown to counter-act extrafoveal/peripheral fading (Martinez-Conde et al., 2006 and Clarke and Belcher, 1962), search and scan micro-displays (Steinman et al., 1973) such as during the task of threading a needle (Ko et al., 2010) and provide cues to the direction of a shift in attention (Hafed and Clarke, 2002). Clearly, motion during fixation is essential to the visual experience. However, it is important to note that too much of this motion could actually deteriorate resolution or impair vision (Burr and Ross, 1982) as well. Therefore, there is an ideal amount of fixational motion necessary for optimal vision.

The power spectrum of fixational eye motion is another method of visualizing and analyzing eye motion data. Typically, motion is graphed as a function of amplitude versus time for a given recording. However, taking the Fourier transform of this data (i.e. converting the time axis into frequency), permits the visualization of the amplitude contribution for each varying frequency component. This allows one to see exactly what frequencies are contributing most to the data. Findlay et al. (1971) was one of the first to show the power spectra of

fixational motion and noted that the amplitude of motion falls off as roughly 1/frequency. Figure 1.2 illustrates this principle.

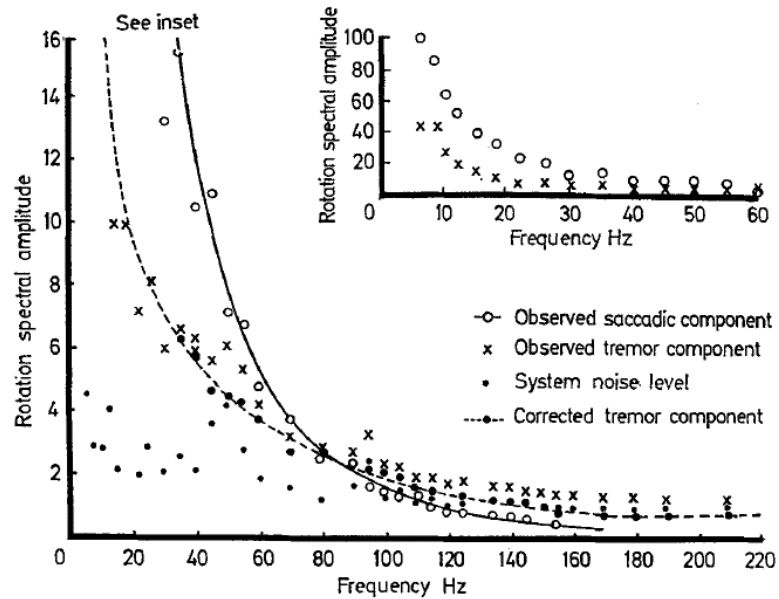


Figure 1.2: Fixational eye motion as a function of frequency depicted by Findlay (1971). Note the different contributions of both saccades and tremor. The units of the abscissa are sec/arcminute (where the square of abscissa gives you power spectral amplitude).

While fixational motion proves useful in preventing the outside world from fading away, it can be a hindrance when performing high-resolution imaging of the retina. Imagine trying to take a fine-detailed picture of a butterfly's wings. If the butterfly is sitting motionless on a flower, capturing the fine detailed pattern on its wings with a single picture is not very challenging. However, if the butterfly is in motion, quickly flapping its wings, a photo may look blurred and poorly resolved due to the constant motion of the object of interest. Taking many more pictures may be necessary, or even an average of multiple pictures, to obtain one worth keeping. The same is true of high-resolution retinal images with fixational eye motion. For a full-field imaging system, image blur can be a big problem. Taking a single snapshot of a moving target, at one instance in time, will likely result in an image that appears blurry, lower contrast, or with motion artifacts. In a scanning system, eye motion will cause actual image distortions. Since the image in a scanning system is acquired pixel by pixel over time, these distortions are similar to those generated when pulling on a piece of paper in the printer while it is still writing. The top (already printed) rows are unaffected by the motion that occurs later on. Similarly, pulling the paper partially out while the machine is actively printing and then stopping, would cause the latter portions of the paper to be preserved. This scenario mimics that of retinal scanning systems, where eye motion can happen during the course of recording a single movie frame. Depending on the type of eye motion that occurs, the resulting images may have portions of the image with shearing, compression, or expansion. The project outlined here aims at designing and building a high-resolution retinal scanning and imaging system paired with

current image-based eye-tracking software to provide extremely accurate eye-tracking and stimulus delivery at a fraction of the cost of Adaptive Optics SLO systems (AOSLO). This system is used as a stand-alone retinal eye-tracker or as an external eye-tracker to drive other high-resolution imaging systems such as AOSLO or OCT.

1.1.2 Current Eye-tracking Technologies and Methods: An Overview

There are generally four categories of eye-tracking that are done for the human eye in modern day research: (1) pupil based eye-tracking (generally referred to as “pupil trackers”), (2) Purkinje reflex based eye-tracking (the most common of these is the Dual-Purkinje system), (3) retinal-based eye-tracking (typically done with SLO systems) and (4) the more invasive, yet highly accurate, magnetic search coil and optical lever methods. The methods listed above in group (4) are capable of recording high fidelity eye motion traces and are generally considered the “gold standard” for measuring fixational eye movements and torsion (more recently, the optical lever method has fallen out of use with the advent of the magnetic search coil method in the 1960’s and 70’s) (Collewijn et al., 1975, Robinson, 1963). Both of these methods rely on the insertion of a contact lens onto the subject’s eye. Attached to the lens is either a magnetic search coil, or in the case of the optical lever method, a mirror. Direct contact with the eye allows for the accurate monitoring of motion, aside from the error due to contact lens slippage. This additional error will contribute an unknown shift in the coil position on the eye, rather than reporting a true fixational eye motion shift. Due to their invasive mounting and recording techniques, search coil methods could potentially lead to subject discomfort and/or corneal scarring and deformation. For primate research, the magnetic search coils are generally sutured directly onto the surface of the eye and therefore do not experience any of the error associated with contact lens movement or slipping. This option, however, is not suitable for human research. Recent studies have brought into question the use of magnetic search coils as the gold standard. Kimmel et al. (2012) reported a 90% agreement between a search coil and the EYELINK 1000 for the recording of fixational eye motion, noting that the search coil accuracy declined slightly as the eccentricity increased. McCamy et al. (2015) found that search coils and the EYELINK 100 video tracking system agreed on 95% of their recorded fixational eye motion. It seems clear that optical eye-tracking techniques have progressed quite rapidly over the last five years.

For the eye-tracking methods described in groups 1-3, their references for motion are based on different portions of the eye’s anatomy. Therefore, there are varying levels of accuracy, resolution and performance for each technology. Depending on the type of eye movement one wishes to study, and the sensitivity of the data that is necessary to obtain, the choice of eye-tracker will make a huge difference. Table 1 showcases the differences between varying eye-tracking technologies. The term “tracking accuracy” refers to the technique’s ability to monitor motion. The larger the number, the less accurate the eye-tracking is. For example, for motion recorded with the TSLO, movement greater than 0.2 arcminutes is accurately captured, while motion less than 0.2 arcminutes falls within the error of the system. “Latency” is the amount of time required to place an external stimulus onto the retina. In the case of the

TSLO, this is the amount of time needed to fully “man” the acousto-optic modulator to scan the laser on the appropriate retinal landmark. This process is further explained in both chapters 3 and 4. Finally, “stabilization accuracy” refers to how stable a stimulus, or other actively steered optical beam, can be placed on the retina.

Table 1.1: Comparison of the TSLO to other current eye tracking modalities

Method	Tracking method	Tracking accuracy	Latency	Stabilization accuracy	Comments
TSLO	Retinal image tracking	0.2 arcmin	2.73 msec	0.66 arcmin	Gaze contingent stimulus projection
AOSLO (Yang et al., 2010)	Retinal image tracking	<0.1 arcmin	3 msec	0.15 arcmin	Gaze contingent stimulus projection. The stimulus is corrected with AO and can be as compact as a single cone.
Optical lever	Direct optical coupling	0.05 arcmin (Riggs & Ratcliff, 1968)	0 (optical)	0.38 arcmin (Riggs and Schick, 1968)	Stimulus is very precise but contact lens slippage will cause uncontrollable and unmonitorable shifts in stimulus position
Magnetic Search Coil	Current signal travels through thin copper wire attached to contact lens	0.5 arcmin (Collewijn, 1975)	0.5 msec (Robinson, 1963)	Not reported	Tracking is very precise but contact lens slippage will cause uncontrollable and unmonitorable shifts in stimulus position
Dual Purkinje (dPi) Eye Tracker with optical deflector (Cornsweet and Crane, 1973)	Purkinje reflexes from cornea and lens	~1 arcmin Crane and Steele (1985)	6 msec	~1 arcmin (error is dominated by tracking accuracy)	Monitors 1 st and 4 th Purkinje reflexes with respect to one another
EyeRis™* (Santini et al., 2007)	dPi**	~1 arcmin	5-10 msec	~1 arcmin (tracking limited) (Rucci et al., 2007)	Gaze contingent display
MP1 (Nidek, Japan)	Retinal image feature tracking	4.9 arcmin (Midena, 2007)	2.4 msec	Not reported	Gaze contingent display for single stimulus presentations (clinical visual threshold measurements)
Physical Sciences Inc. (Hammer et al., 2006)	Retinal feature tracking	3 arcmin	< 1 msec	3 arcmin (tracking limited)	Used optical hardware to maintain a scanning raster on its intended retinal location to facilitate high fidelity line scanning ophthalmoscope imaging.
Heidelberg Spectralis OCT(Heidelberg, Germany)	Retinal image feature tracking	Not reported	Not reported	Not reported	Used optical hardware to maintain an OCT B-scan at its intended retinal location to facilitate scan averaging and high fidelity volume imaging.
Eyelink 1000*** (2000 Hz monocular, 1000 Hz binocular)	Pupil tracking	15-30 arcmin	1.4 - 3 msec	Not reported	Monocular and binocular pupil tracking with a head mounted video-based eye tracking system.

Adapted from Sheehy et al., 2012

* This technique falls into a broad class of eye trackers coupled with gaze contingent displays. The EyeRIS system here has the best reported performance of any of the systems we found.

** Any tracking method can be used for this type of system but results from dPi system are reported since they provide the best results.

*** There are many head mounted video based tracking systems used for psychophysical experiments, but the Eyelink brand is the most commonly reported system (28 out of 31, or 90% usage) for experiments measuring human microsaccades in a recent review (Martinez-Conde et al., 2009).

One important question to ask is how does the TSLO compare with other current tracking technologies? The TSLO fares well compared to other tracking methods, with only the AOSLO and the invasive optical lever/magnetic search coil methods showing greater accuracy. However, it is important to keep in mind that the tracking capabilities of the TSLO are an extension of those first reported for the AOSLO. The greater accuracy of the AOSLO does come at a cost. The smaller field size of the AOSLO has two main consequences. First, the same lateral motions in a small-field system cause a greater loss of overlap with the reference frame, resulting in a larger number of tracking and stimulus delivery failures due to sub-threshold cross-correlation peak values. Second, the threshold velocity is lower for the smaller field sizes. Additionally, the AOSLO stimuli are limited in their extent due to the small scanning raster of the system (1° - 3°). Therefore, while the increase in field size of the TSLO has lower tracking accuracy, the payoff is fewer software failures caused by larger eye motions, which leads to a more robust performance. In terms of the optical lever/search coil methods for stimulus control, slippage of the contact lens causes ambiguity in stimulus placement, leaving an uncontrollable amount of retinal movement directly affecting stimulus placement.

For the monitoring of larger eye-motion, such as saccades, smooth pursuit, and the occurrence/timing of microsaccades, pupil-trackers are the best fit. Additionally, these eye-trackers tend to be “wearable” systems, giving the investigator more freedom for experimental design. However, these systems do have some shortcomings. First, accurate calibration is needed at both the beginning and end of an experiment. This is generally done by mapping the pupil locations while the subject views 6-9 stimuli on a monitor or screen. Next, pupil tracking performed during tasks, such as viewing a movie with changing luminance values, can result in an error of reported pupil location of up to 2.5° if not compensated for (Choe et al., 2015, Drewes et al., 2014, Drewes et al., 2012). Additionally, the temporal response of the system may be limited due to its video-based scanning. Finally, the smallest motion that can be accurately detected is roughly 15-30 arcminutes, or $\sim 0.25^\circ$ - 0.5° . This means that much of the motion made during fixational drifts falls within the noise of the instrument. One of the most common pupil tracking systems used in the research domain is the new Eyelink 1000, which is the updated model of the previously used Eyelink II. Figure 1.3 showcases this wearable head-mounted technology with individual cameras pointed at each eye.



Figure 1.3: Eyelink II pupil eye-tracking system. Both right and left pupils are monitored with individual cameras. Accuracy of down to 30 arcminutes is expected, with the new Eyelink 1000 system having an accuracy of down to 15 arcminutes. <http://www.sr-research.com/eyelinkII.html>

The varying reflections from the optical surfaces of the eye are known as the Purkinje reflexes. There are four reflections that occur within the eye: the front surface of the cornea (P_1), the back surface of the cornea (P_2), the front surface of the lens (P_3), and the back surface of the lens (P_4). These are illustrated in figure 1.4a. A Dual-Purkinje (dPi) eye-tracking system uses light reflected from the front surface of the cornea (P_1) and the rear surface of the lens (P_4) at the interface with the vitreous humor. The placement of the reflections with respect to each other (or their separation), as well as how they move compared to one another, gives the necessary information to monitor translation, rotation, and angular orientation of the eye. When the eye experiences translation, usually due to head motion in the lateral direction, the 1st and 4th Purkinje images will move the same distance in the same direction. If the eye undergoes rotation however, the two images will change their separation proportionally to the angle of rotation.

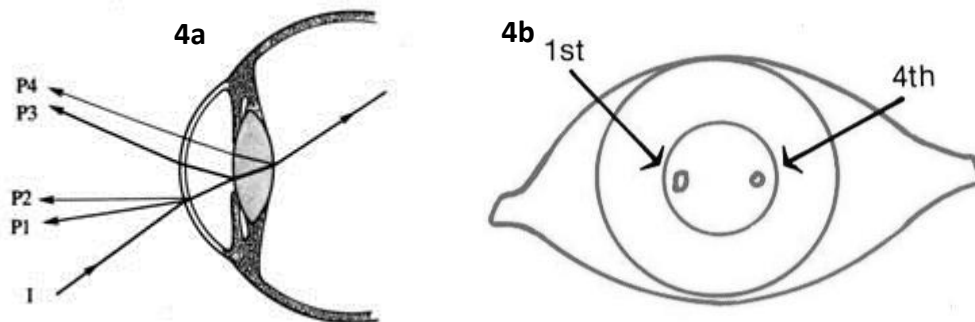


Figure 1.4: a) a diagram showing the four Purkinje reflexes from their corresponding optical surfaces. b) A frontal view of P_1 and P_4 – the reflexes used for Dual-Purkinje eye-tracking. <http://ppw.kuleuven.be/home/english/research/lep/resources/purkinje>

Dual-Purkinje systems are generally used in research lab settings. They have an accuracy of 1 arcminute and are capable of delineating rotational versus translational motions of the eye. If monitoring rotation or lateral head translation is important to the experiment, then these systems are a good choice. Additionally, an accuracy of ~1 arcminute is capable of fixational eye motion monitoring. Currently, these systems are manufactured by Fourward Optical Technologies for \$60K in the US and \$65K internationally. The main issues that arise during the use of these systems, as well as with the Eyelink systems, is that there is no record of exactly what portion of the eye is being used to view a stimuli and no unambiguous record of where a stimuli landed. Additionally, dPi system latency runs at about 6msec, making external tracking capabilities with high-resolution imaging instruments difficult due to this delay.

Ophthalmoscopic systems are commonly used for retinal eye-tracking. Cornsweet was the first to implement retinal eye-tracking techniques through the use of such a system (Cornsweet, 1958). He used a spot of light that was scanned over a subject's optic-disc at a scan rate of $< 20\mu\text{sec}$. Light reflected from the eye was detected on a PMT and the output was viewed on an oscilloscope. During a task of fixation, he noted that if the eye moved between scans, a displacement of the scans could be seen. This shift in the position of the trace could then be directly attributed to the movement of the eye. The system had an accuracy of 10 arcsec and could record motion as large as 3 or 4 degrees. While Cornsweet later went on to develop the dPi eye-tracking systems, other scientists and researchers continued to use ophthalmoscope systems to monitor eye motion. Hammer et al. (2003) used a dithered probe beam in a line scanning system to lock onto the lamina cribrosa of the optic disc to track retinal motion with an accuracy of 3 arcminutes. By capturing the motion of blood vessels, and other easily trackable retinal surfaces, off-line tracking was performed in the late 80's and early 90's to extract the motion of the eye (Ott and Eckmiller, 1989, Schuchard & Raasch, 1992, Ott & Daunicht, 1992, Lakshminarayanan et al., 1992). Stetter et al. (1996) developed a method to extract horizontal eye motion from an SLO with high temporal resolution, followed soon after by Mulligan (1997) who later refined this for motion in the vertical meridian as well. Since an SLO image is captured sequentially, Mulligan used biquadratic interpolation to determine cross-correlation maximums between an input image and a reference template with subpixel precision. This enabled the extraction of eye motion data with a resolution of better than 1 arcminute.

In summary, there are a variety of eye-tracking systems available for researchers. It is ultimately up to the investigator to choose which type of system best achieves their experimental goals. SLO tracking systems are great tools to not only record eye motion, but also to actively visualize exactly what part of the retina is being used for a particular task.

Chapter 2: Optical Design and Modelling of the Tracking Scanning Laser Ophthalmoscope

2.1 Abstract

A tracking scanning laser ophthalmoscope (TSLO) system was designed using an out-of-plane configuration (Gomez-Vieyra et al., 2009) over an 8° FOV. Through the use of a 90° mirror folding configuration, system wavefront RMS was improved by an order of magnitude compared to planar configurations (Gomez-Vieyra et al., 2009). Additionally, astigmatism over the entire field of view, as well as angle-dependent aberrations, were minimized by reducing the angles of incidence on the telescope pairs. Performance characterization and optimization was completed over the entire scan field using ZEMAX to verify best optical set-up and angle of incidence for each optical element. Beam profiles at 840 nm for both the pupil and retinal planes were evaluated for a 4 mm system pupil size. The opto-mechanical design was completed using Solidworks in order to choose optimal vendors and components. Overall, diffraction-limited system performance was achieved for all nine scan configurations spanning the 8° FOV.

2.2 Introduction

The TSLO system design was modelled from established AOSLO designs used within the Roorda laboratory (Roorda et al., 2002). The system contains a series of concave mirrors in afocal telescope arrangements to relay the pupil of the eye onto both a horizontal and vertical scanner and then to a light capturing device, or PMT. Historically, system designs included the horizontal tilting of concave mirrors to relay light through the optical elements in a single plane. This tactic of consistently adding horizontal angles to propagate light adds a large amount of astigmatism into the system. This can prove detrimental in system design, as one generally wants to limit excess aberrations in order to optimize diffraction-limited performance. To combat this issue in the TSLO design, an out of plane design was chosen, with the tilting of curved mirrors in both the x and y directions, in order to compensate for system astigmatism and limit overall aberrations (Gomez-Vieyra et al., 2009).

2.3 Methods

2.3.1 Optical Design and Optimization of the Tracking Scanning Laser Ophthalmoscope

For the design of both AOSLO and TSLO systems, there are typically two optical planes to pay close attention to for performance metrics: the pupil planes and the retinal planes. In the TSLO system, pupil conjugates are located at the entrance pupil of the system, at the plane of the horizontal scanner, the vertical scanner, and at the human subject's pupil. Since the curved mirrors in the front end of the system are set up as afocal telescopes (with a separation equaling the sum of their focal lengths), the retinal planes are located at the focal point between each set of curved mirrors, the human subject's retina and at the pinhole just prior to the PMT. The use of this pinhole is what makes the TSLO confocal – rejecting light from

unfocused retinal planes. For most studies performed, the desired plane of focus is the photoreceptor layer.

In order to limit system astigmatism within the pupil planes of the TSLO system, the following equation must be met (Gomez-Vieyra et al., 2009):

$$I_2 \approx \sqrt{-\frac{M}{\cos(2\theta)}} I_1. \quad (1)$$

Where I is the angle of incidence of the principal ray onto the mirror, M is the telescope magnification and θ the orientation of the plane that is defined by the principal ray and corresponding marginal ray. Note that for $\theta = \pi/2$, or a perpendicular plane orientation, this produces the most compact optical layout which ultimately leads to smaller angles of incidence. Similarly, the condition for minimizing astigmatism in the retinal plane is:

$$I_2 \approx \sqrt{\frac{1}{M \cos(2\theta)}} I_1. \quad (2)$$

By comparing both equations (1) and (2), it is clear to see that the only way system astigmatism can be minimized in all telescopes for both pupil and retinal planes is when M is equal to one. Additionally, smaller angles of incidence for all configurations should be utilized when possible. Ideally, these equations are used when determining system angles of incidence, as well as optimal mirror focal lengths. However, when actually designing a system to build, the limiting factors in determining the smallest angle of incidence possible are typically the optical mounting and mechanics. Therefore, these equations approximate the angles of incidence before necessary scaling is needed to fit in the appropriate optomechanics. Figure 2.1 shows the ZEMAX (Radiant ZEMAX LLC, Bellevue, WA) design for the front end of the TSLO system. A good rule of thumb is to keep the angles at a minimum.

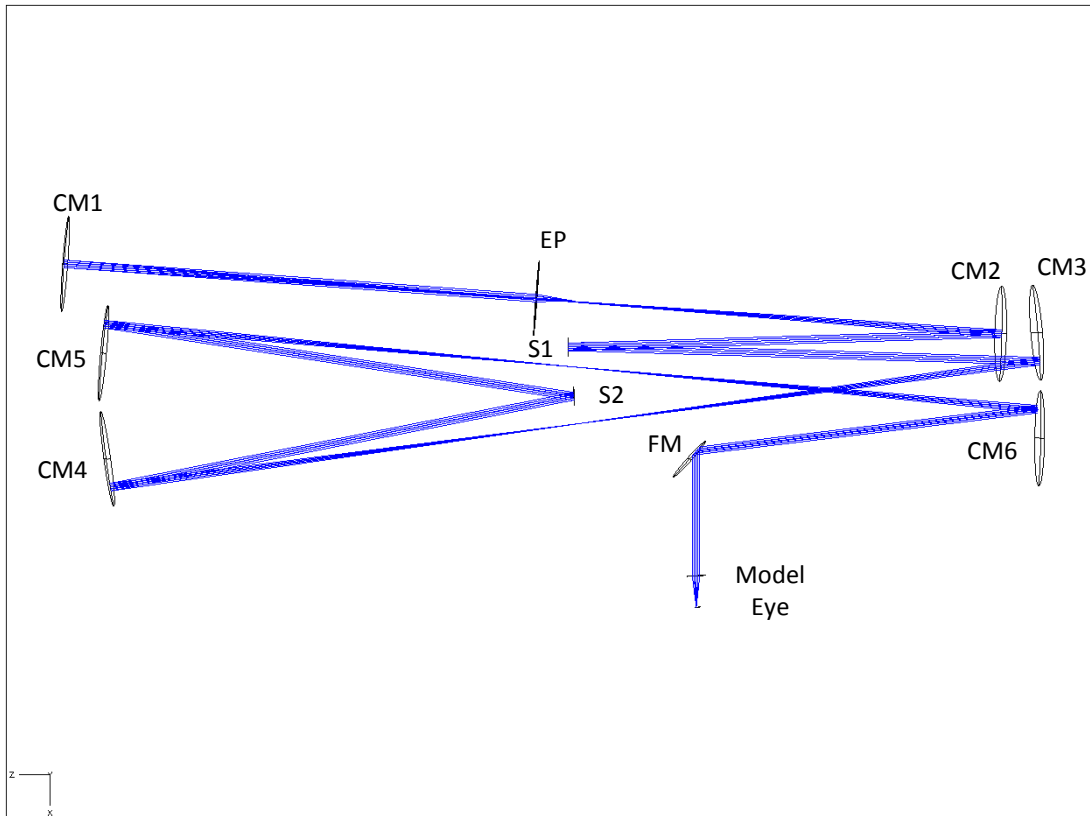


Figure 2.1: Front-end ZEMAX design of the TSLO system. The beam is relayed through a series of three off axis telescope assemblies, each containing two concave mirrors with a focal length of 250 mm, and onto the model eye. Both scanners (S1 – resonant scanner and S2 – galvo scanner) are placed at pupil conjugates.

The performance of the system was then modelled utilizing the multi-scan configuration option in ZEMAX to simulate the entire scan field. This option allows one to model multiple positions for both the horizontal and vertical scanning mirrors within the system. In doing so, performance can be determined over the entire scan field, as well beam characterization in particular locations of the scan. Optimization of the design was then performed directly in ZEMAX using the “optimization” function. This iterative process uses the merit function to best determine the lowest RMS wavefront values possible for each configuration. In total, nine points at $\pm 4^\circ$ from the center of the field were modelled. The distribution of light intensity in the image plane for each location was then plotted. Figure 2.2 shows the spread of the beam for all scan angles within the calculated diffraction limited airy disc for a 4 mm pupil at a wavelength of 840 nm. Indeed, all of the spots fall well within the diffraction limit, with the central field having the least amount of aberration.

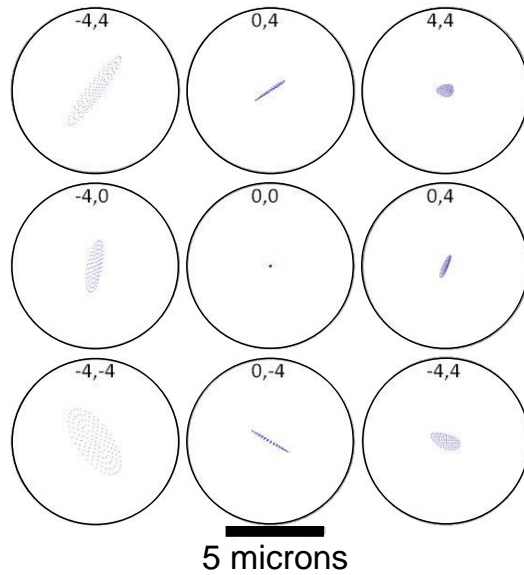


Figure 2.2: Geometric spot diagrams contained within the calculated Airy discs at nine points spanning the 8° FOV ($\lambda = 840 \text{ nm}$ with a pupil size of 4 mm). The coordinates represent the (x,y) field location in degrees.

The pupil planes of a scanning system, or the back focal plane of the second mirror in an afocal telescope pair, contain the stationary point of the beam. This “pivot point” is relayed onto each scanner and the human eye. Many times while optimizing an optical system, attention is paid solely to image plane metrics to determine beam quality and performance. However, aberrations play a large role in pupil plane optimization as well, as they could cause the PSF of the beam to translate or broaden laterally due to the scanning nature of the system. In the literature, this phenomenon is termed “beam wandering.” Maintaining a stationary pivot point is important since it allows us to position the beam at the point in the eye’s optics with the least aberration. Limiting system astigmatism can greatly reduce this performance deterioration. To address this issue, each telescope pair can be modelled in Zemax in series as if a point of light is diverging from the system’s entrance pupil. This allows one to find the optimal distances to separate each set of telescopes. Figure 2.3 shows an example of what the beam wandering looks like for an optimized 8° FOV TSLO system. From this figure, it is apparent that beam wandering cannot be completely eliminated, but proper optical design allows for the minimization of this phenomenon.

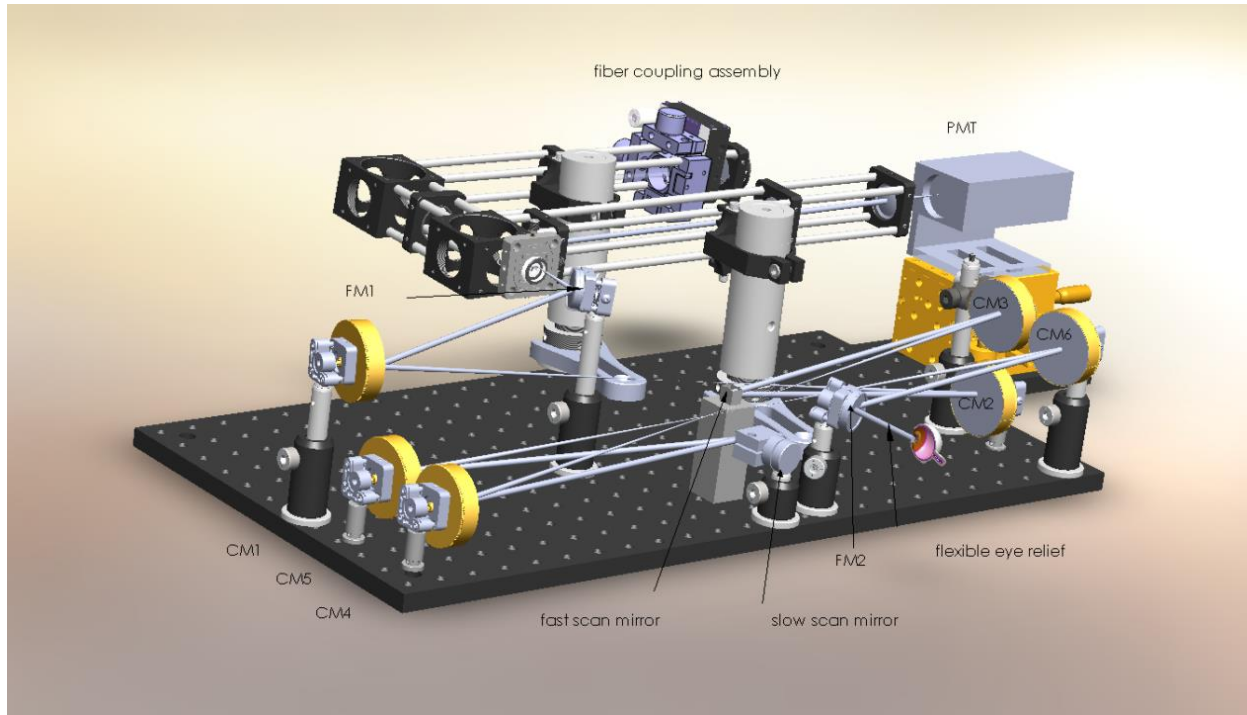


Figure 2.4: Optomechanical design of the TSLO system as modelled in Solidworks.

2.4 Results

The tracking scanning laser ophthalmoscope (TSLO) system specifications are as follows:

- Diffraction-limited optical design over an 8° FOV (excluding the eye)
- Adjustable pupil size between 2-4 mm (no need for subject dilation)
- Small focal length mirrors for a compact design
- Flexible eye relief

The main portion of the system contains three telescope assemblies that relay the pupil to the fast and slow scan mirrors and then to the light detection arm. The telescopes are arranged in such a way so as to minimize astigmatism in both the pupil and retinal planes. Each concave mirror has a focal length of $f = 250$ mm. A pinhole is placed at the retinal conjugate prior to the photomultiplier tube (PMT) in order to make the system confocal. A galvo scanner and resonant scanner are placed into the system at pupil conjugate positions to scan the beam across the subject's retina both vertically and horizontally, respectively. The horizontal, or fast, scanner operates at ~ 16 kHz, while the vertical scanner operates at a rate of $1/512^{\text{th}}$ of the fast scan to record frames at ~ 30 frames per second. An image is created, pixel by pixel, with each frame consisting of 512×512 pixels. Since each video frame is acquired over time, there are a unique set of distortions created by the subject's eye motion. It is these distortions that are used to extract the motion of the eye in real time. Figure 2.5 shows a schematic of the system.

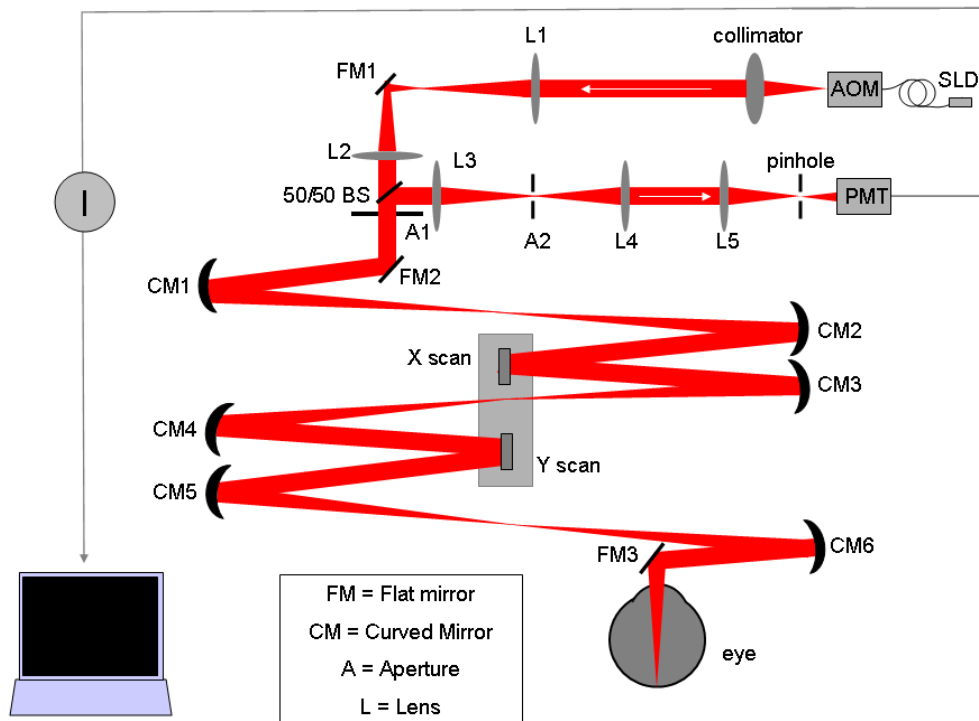


Figure 2.5: A 2-D optical design schematic of the TSLO. Light exiting the super luminescent diode (SLD) is coupled into the acousto-optic modulator (AOM) before entering the system. The light is collimated and sent through a basic 4f series of lenses onto an adjustable aperture (A1). Light travels through three mirror based telescope assemblies ($f = 250$ mm) to the human eye. Light is then reflected off the retina and sent back through the system into the light detection arm. Another series of lenses in a 4f configuration relays the light to be collected by a photomultiplier tube (PMT). A $50 \mu\text{m}$ pinhole (1.95 Airy disc diameters for a 4mm pupil) is placed at the retinal conjugate plane prior to the PMT for confocality. The intensity (I) of the signal is sent to the PC for readout. This is a schematic layout; the actual components are not aligned in a single plane.

2.5 Discussion

The TSLO out of plane system design utilizes state-of-the-art optical design principles that are currently employed in advanced AOSLO system designed to visualize foveal cones and rods. While the TSLO system does not have AO capabilities, with the proper optical design, alignment and maintenance, it can still achieve high-resolution retinal images over a larger field than just AO alone.

One important aspect of the TSLO system design is the chosen FOV. Optical design was completed for an 8° FOV, but practically a field size of $1\text{-}5.5^\circ$ is commonly used within the laboratory based on mechanical constraints. However, this FOV can be made larger by the simple adjustment in focal length of the final curved mirror in the last telescope of the system prior to the eye. Swapping out a lens or mirror with a smaller focal length than the current 250

mm focal length mirrors, increases the FOV. This is due to the fact that system magnification and field of view are inversely proportional. For example, the current system design has a final telescope with both CM5 and CM6 equal to 250 mm. If a 125 mm focal length mirror or lens is substituted for CM6, the beam size will be equal to $\frac{1}{2}$, but the FOV will increase 2-fold. One might then prefer to have a mirror or lens carousel as the last element, allowing for multiple field of view options. This would give the TSLO far more utility, as a larger field of view can capture larger fixational eye motion, while a smaller field allows one to really take advantage of the system resolution.

Another important aspect of the system is its pupil size. The optical design was optimized for a 4 mm pupil, which means this aperture size (and below) are suitable for operation. Therefore, the TSLO is capable of having a flexible system entrance pupil anywhere between 2 - 4 mm. This is beneficial for two main reasons: (1) dilation is not required for subject/patient imaging and (2) pupil size can be adjusted anywhere from 2-4 mm on a subject-to-subject performance basis (Donnelly et al., 2003). For point 1, not having to use dilation drops eliminates time, safety concerns and ease of use constraints. For the second point, the experimenter has the flexibility to make the system pupil size smaller for those subjects with poorer optics and/or smaller human pupil sizes, which is common for the aging population.

2.6 Summary

A compact, easy to use, and cost-effective system was designed to implement as an image-based eye tracking system. Optical design in ZEMAX showed diffraction-limited system performance for the 840 nm light and 4 mm system pupil size. Mechanics were modelled in Solidworks to ensure compact system design and ease of future integration with external systems.

2.7 Acknowledgements

A portion of the work described in this chapter, namely sections 2.32, 2.4 and 2.5 were published as a first-author manuscript in *Biomedical Optics Express* in September of 2012. Alfredo Dubra is thanked for helpful conversations regarding out-of-plane SLO design considerations. The author would also like to thank Pavan Tiruveedhula for his superior work on the electronics and software portion of this system. This research was supported by grants from the National Institutes of Health EY014735 (AR, DWA, QY), the University of California, Berkeley Vision Science Graduate Student Training Grant T32EY007043 (CKS) and the Macula Vision Research Foundation (AR, CKS).

CHAPTER 3: Real-time Eye-tracking with the TSLO

3.1 Abstract

This chapter discusses the ability of a high-speed, image-based tracking scanning laser ophthalmoscope (TSLO) to provide high fidelity structural images, real-time eye tracking and targeted stimulus delivery. The system was designed for diffraction-limited performance over an 8° field of view (FOV) and operates with a flexible field of view of 1 - 5.5°. Stabilized videos of the retina were generated showing an amplitude of motion after stabilization of only 0.2 arcmin or less across all frequencies. With a smaller field size of 2°, individual cone photoreceptors were clearly visible at eccentricities outside of the fovea.

3.2 Introduction

With the eye as an ever-moving target, the ability to record high-fidelity images of the retina is limited. Moreover, targeted light delivery to the retina remains uncontrolled with constant eye motion. Recent advances in imaging technology have highlighted the importance of improved eye tracking to render true and accurate images. In the clinical domain, active eye tracking has proven to be effective in commercial systems (Sadda et al., 2010, Garcia-Martin et al., 2012). At a more basic level, the benefits of accurate eye tracking and stimulus delivery prove to be useful for delivering stimuli to targeted retinal locations as small as a single cone (Sincich et al., 2009).

An image-based method for eye tracking and targeted stimulus delivery has been implemented into an adaptive optics scanning laser ophthalmoscope (AOSLO) system and has been reported in a series of publications (Vogel et al. 2006, Arathorn et al. 2006, Yang et al. 2010). This chapter demonstrates that the same image-based tracking techniques can be implemented in a more traditional, larger field of view, confocal SLO. This system is the most accurate, fast and functional tracking system used in a standard ophthalmic instrument and demonstrates that rich texture in the image, not necessarily the presence of cones, is sufficient for this tracking method. The use of a conventional approach offers a more robust, compact and cost effective system that is readily deployable in a variety of settings. In a well-designed SLO system, the wider field of view (FOV) is able to capture retinal video rich with structure, allowing accurate image-based tracking during normal fixational eye movements.

3.3 Methods

3.3.1 Overview of Eye-tracking Software

The details of the eye motion recovery used in this system have been previously reported (Arathorn et al., 2007, Yang et al., 2010, Mulligan, 1997). Briefly, the methods are described herein. In order to extract retinal motion from the scanned images in real time, each frame of an SLO movie is broken up into a set number of strips that are parallel to the fast scanner. The number of strips is flexible and can be changed according to the user's

experimental requirements. For each movie, a reference frame is selected, usually the first frame to occur in the series unless otherwise reselected. Each strip within a given frame is then cross-correlated with the reference frame. The (x,y) displacements of the new frame with respect to the reference frame are a measure of the relative motion of the eye at that specific point in time. Every subsequent frame can then be redrawn to align it with the reference frame (Figure 3.1). This occurs in real-time so that the operator can see both the subject's actual retinal motion and the stabilized version of the retina side by side on the software interface. Using the real-time eye trace generated from the (x,y) displacements of each frame as described above, the timing of the stimulus delivery can be controlled to guide its placement to any targeted location on the retina.

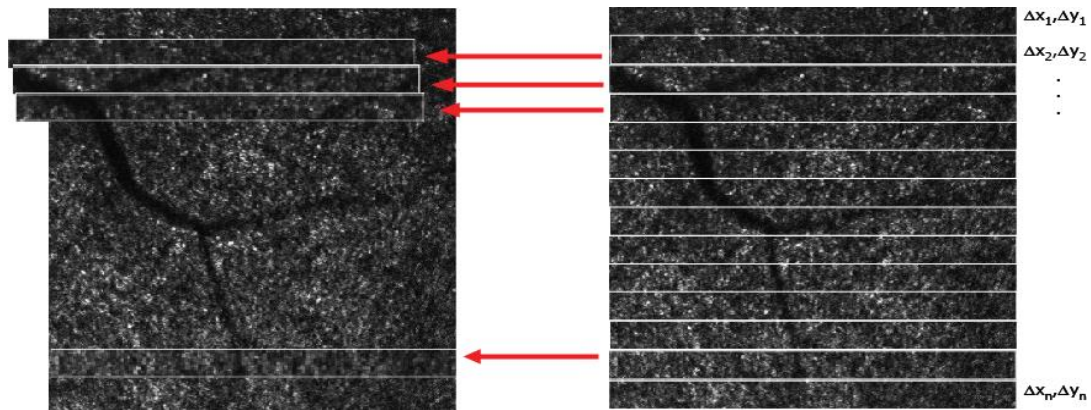


Figure 3.1: Recovery of eye motion. Each frame is broken into strips that are cross correlated with the reference frame (left) in order to determine the (x,y) displacements. In the current implementation, these cross-correlations are made to the nearest pixel.

For the data presented here, cross-correlations are performed and (x,y) displacements are reported 32 times per frame, for a reporting rate of 960 Hz. The correlations are computed from 32 overlapping strips per frame, each of which is 32 pixels high. Eye position estimates are made after-the-fact (i.e. after the strip has been recorded). This computation is done very quickly, but the delivery of a stimulus to a targeted retinal location requires a prediction as described in Chapter 4. Briefly, for a 16 kHz line scan rate, the latency is 2.5 +/- 0.5 msec, depending on where in the 16-pixel strip the stimulus actually starts.

3.3.2 Frequency Analysis Using Both a Model and Human Eye

Detailed tracking performance was quantified on a custom-built model eye, which used a galvo scanner mirror placed between the optics and the retina. This allowed for controlled amounts of retinal motion with fixed frequencies and amplitudes. Human eye data are reported here for two subjects. The experiment was approved by the University of California, Berkeley, Committee for the Protection of Human Subjects and all protocols adhered to the tenets of the Declaration of Helsinki. A chin rest with temple pads was used in order to minimize head motion for all human eye experiments. All measurements were recorded with a 4° FOV (512 x

512 pixels) providing a sampling resolution of 0.47 minutes per pixel. The power of the 840 nm light source never exceeded 500 μW at the pupil plane, which was computed to be within the ANSI safety limits (ANSI, 2014).

To quantify motion reduction as a function of frequency, sinusoidal retinal motion was input into the model eye. Both a raw video and stabilized video were recorded at each input frequency. An offline stabilization program was used to compute retinal motion in the raw and stabilized video (Stevenson et al., 2010). The offline software generated eye motion estimates at a frequency of 1920 Hz (64 strips per frame). The amplitude spectra were then computed for both eye motion traces and the amplitudes of each spectrum at the input frequency were compared before and after stabilization. In this manner, any residual motion in the stabilized video that was not corrected by the real-time system could be measured. Eye motion measurements were recorded at nearly 100% accuracy for frequencies up to 32 Hz (Figure 3.2). The estimated bandwidth for 50% correction based on a double exponential fit to the data was just over 400Hz.

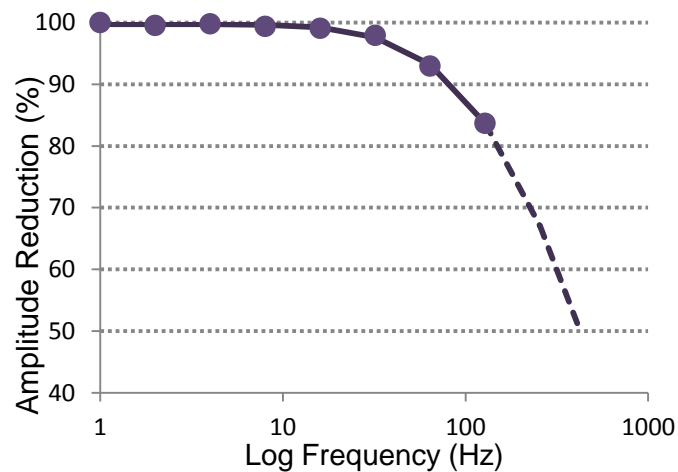


Figure 3.2: Motion amplitude reduction as a function of input frequency for the model eye. For input frequencies just over 100 Hz, the reduction in amplitude is still over 80%.

Next, raw and stabilized videos were taken of the human retina in real time. Ten videos of ten seconds each were recorded of one of the subjects. The same offline stabilization program with increased sampling was used for the human eye videos. The percentage of erroneous eye motion estimates was 0.83%. The standard deviation of the residual motion of features in the stabilized videos was 0.19 minutes of arc (0.41 pixels). The amplitude spectra of motion as a function of frequency shows how the actual motion in the human eye is corrected in this system. Figure 3.3 shows two important results. First, eye motion of a normal eye fixating on a target is dominated by low frequencies, with the amplitude dropping with the frequency (Stevenson et al., 2010). At frequencies greater than 10 Hz, the amplitude of normal fixational eye motion is less than 0.5 arcminutes. Second, the TSLO suppresses the eye motion

during normal fixation up to 100 Hz. The suppression of eye motion in the stabilized video means that eye motion is being reliably measured over these frequencies in real-time.

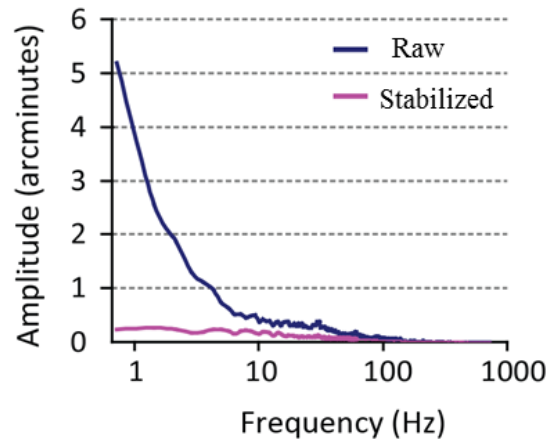


Figure 3.3: Amplitude of eye motion vs. frequency. The blue curve represents the actual motion as a function of frequency during normal fixation recorded in the raw video. The pink line represents the residual motion of features in the retinal video after stabilization. The resultant amplitude with stabilization is 0.2 arcminutes or less across all frequencies.

3.3.3 Software Velocity Threshold Calculations

The system’s maximum tolerable velocity was computed in order to determine how fast an eye movement can be tracked without software failure. A triangular wave input was fed into the galvo scanner of the model eye and amplitude was increased (velocity increased) to the point where the tracking began to fail. These failures occur because, at high velocities, the shear of the features within a strip causes the height of the normalized cross-correlation with the reference frame to go below the 0.3 threshold level (see section 2.2). The corresponding threshold velocity was found to be 1761 pixels/sec. Since the velocity of motion in pixels is inversely proportional to the field size, the velocity threshold in degrees per second will depend on field size. Equation 1 establishes this relationship:

$$VelocityThreshold = 3.44 \times FieldSize \quad (3)$$

where *VelocityThreshold* is the maximum trackable velocity in degrees per second and *FieldSize* is the TSLO field size in degrees. According to this equation, a field size of just over 5.2° would be required in order to correct for the median microsaccade velocity of ~18 °/s (Engbert and Kliegl, 2003, Martinez-Conde et al, 2004). For this metric, the larger field size of the TSLO over that previously reported with the AOSLO with a maximum field size of ~2°, offers a performance advantage.

3.3.4 System Resolution

Although this system was designed to be of a wider field size than the typical 1-3 degree field of view of the AOSLO, the field of view may operate anywhere from 1-5.5°. By adjusting the angles of each of the scanners, the field size can be made smaller in order to determine the finest structures resolvable. With a 2° field of view, photoreceptor structure starts to become visible outside of the fovea region, with a clear photoreceptor mosaic seen at 4° and beyond without the use of adaptive optics (figure 3.4).

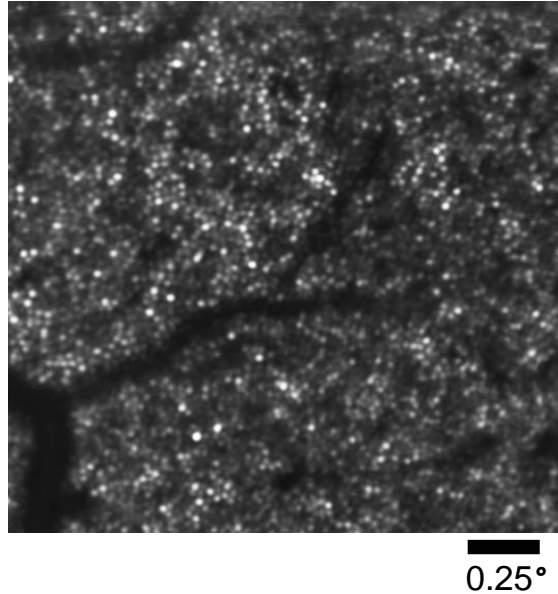


Figure 3.4: Image of the cone photoreceptor mosaic of an emmetropic eye at 4° eccentricity from the fovea. The image is an average of 300 stabilized frames from a single 10-second stabilized video. The bright white circles are individual cone photoreceptors, while the dark shadows extending from the lower left corner into the center of the image are blood vessels.

3.5 Discussion

The TSLO is a robust, high speed, image-based retinal eye tracker that is adaptable to both clinical and research settings. The system may serve as a stand-alone system for recording and stabilizing retinal movies in real-time, as well as providing targeted stimulus delivery for psychophysical experiments. A potential application of the TSLO is that it can be coupled with a variety of other systems that are in need of accurate eye tracking. These systems include OCT, AOSLO, mere and laser guided surgery. The use of the TSLO coupled with these technologies will render high fidelity images without excess motion artifacts, as well as provide an unambiguous record of stimulus delivery onto the retina.

While it is clearly shown that the TSLO has many advantages over other tracking technologies, it is important to also understand its limitations as well. First, the reference frame itself will have distortions due to eye motion. Since each frame is built up pixel by pixel,

each frame in a movie has unique distortions. Once a reference frame is selected, every subsequent frame will then be stabilized against it. The selection of a reference frame is done manually, using a button press directly in the software interface. If the reference frame is selected during a large microsaccade or blink, the video will not be able to stabilize properly in real-time, revealing a warped stabilized video. In these situations, the operator has immediate visual feedback on the choice of a reference frame and can always reselect whenever necessary during an imaging session. Second, vertical shifts of the eye can cause a loss of retinal information for eye tracking. Currently, a single frame is used as the reference frame to compute eye motion. If the eye moves vertically, there will be strips that do not overlap with the reference. The TSLO does offer a larger FOV than the AOSLO (currently operating at 5.5° compared to the typical AOSLO usage of $1-2^\circ$), which allows one to accurately capture more retinal structure. While this proves highly beneficial for horizontal motion, it still produces error in the vertical direction. Lastly, only eye motions that cause horizontal and vertical displacements of the retina are computed. Rotations of the eyeball about its optical axis, or torsion, are not corrected for properly. The correction of torsion is possible, but the extra computation time needed for its contribution outweighs the benefits of correcting the motion in real-time. It should be noted that even though these errors add artifacts to the eye motion trace, they do not preclude accurate placement of a stimulus at the targeted location.

3.6 Summary

The TSLO is a high speed, robust eye tracking system that provides high-resolution retinal images. It has been shown that the FPGA solution, with FFT-based cross correlation algorithms, can be translated to traditional scanning laser ophthalmoscope technology. The use of this technology will provide a more compact, robust and cost-effective solution for the study of the retina and fixational eye movements. Using smaller fields of view outside of the foveal region showcases the system's single cell resolution, with individual cone photoreceptors clearly visible without the use of adaptive optics.

3.7 Acknowledgements

The efforts described in this chapter were published as a first-author manuscript in *Biomedical Optics Express* in September of 2012. Some of the research was performed at the Rotterdam Ophthalmic Institute with assistance from Kari Vienola, Boy Braaf and Koenraad Vermeer. Scott Stevenson and Girish Kumar provided the offline motion analysis software. This research was supported by grants from the Macula Vision Research Foundation (AR, CKS), the National Institutes of Health EY014735 (AR, DWA, QY), T32EY007043 (CKS), Stichting Wetenschappelijk Onderzoek Oogziekenhuis Prof. Dr. H.J. Flieringa (SWOO) and the Combined Ophthalmic Research Rotterdam (CORR). A special thank you to Austin Roorda, Kate Verhoef and Johannes de Boer for allowing me to come/stay in Rotterdam, Netherlands and work at the Rotterdam Ophthalmic Institute to perform a portion of the results highlighted here.

CHAPTER 4: Microperimetry Using the TSLO System

4.1 Abstract

Chapter 4 demonstrates the visual function testing capabilities of a tracking scanning laser ophthalmoscope system. The TSLO system, which has been described in previous publications, uses image-based eye-tracking to track the retina in real-time with an accuracy of 0.20 arcminutes. With the addition of stimulus delivery arm ($\lambda = 532$ nm), functional testing was performed on one patient with diagnosed toxoplasmosis scarring and one patient with a subclinical unknown retinal pathology. Visual sensitivity was measured using a 40-trial QUEST staircase with a yes/no response paradigm. Each location was tested three times. Increment stimulus delivery accuracy matches that for decrement stimuli with a TSLO system (an average of 0.66 arcminutes), with the exception of the additional error due to the transverse chromatic aberration difference between the imaging wavelength ($\lambda = 840$ nm) and the stimulus wavelength ($\lambda = 532$). This was measured to subjectively be 0.28 arcminutes/degree (Thibos, 1987) and objectively to be an average of 0.21 arcminutes/degree (Winter et al., 2015).

4.2 Introduction

Microperimetry is the pairing of retinal imaging (structure) and functional testing. Most typically, fundus-based imaging is done in order to look for and observe structural changes or abnormalities within the retina. Functional testing can then be performed on areas of interest by determining the necessary light levels (or thresholds) needed for a patient to see a stimulus. However, functional testing has lacked the necessary repeatability and reliability to hit specific retinal locations due to the always present fixational eye motion. There are currently no commercially available systems that allow an experimenter to know exactly what part of the retina they are targeting and be able to repeat a future experiment at that location. Systems like the MP1 (Nidek Technologies, Padua, Italy) utilize a crude eye-tracking algorithm at 30 Hz to perform a frame-by-frame comparison of eye motion. While this is a helpful improvement, a lot of motion can occur during the recording of a single frame, leaving ambiguity in stimulus placement and repeatability. These systems report a mean eye-tracking accuracy of 4.9 arcminutes, with registration errors between eye-tracking images and fundus photos of up to 2° (Enoch et al., 2004, Woods et al., 2007). Therefore, there is still much ambiguity in the structure/function relationship in retinal pathologies. This predicament clearly outlines the need to develop a system with reliable eye-tracking capabilities and precise and accurate stimulus delivery.

AOSLO systems have been previously used for functional testing at the level of single cone photoreceptors. Using a combination of their exquisite high-resolution imaging capabilities, and the same eye-tracking software techniques described in Chapter 3 for the TSLO, they report a stimulus delivery accuracy for $\lambda = 680$ nm of 0.81 arcminutes in the vertical meridian and 0.89 arcminutes in the horizontal meridian (Tuten et al., 2012). While being able to probe and elicit responses from fully resolved single cones using AO makes a profound contribution to basic science, for clinical applications this level of accuracy may not be

necessary, especially at its current price point of \$250K. This is where the TSLO system has the ability to offer high accuracy and repeatability of stimulus delivery, at an affordable price point and an easier to use system set-up.

This chapter details an addition to the current TSLO system that allows for the delivery of both increment green light stimuli ($\lambda = 532$ nm) and decrement stimuli (black on a red background) for sensitivity and threshold testing on patients with retinal pathology, as well as subjects with normal vision. Clear differences in threshold values existed between areas of complete vision loss, or scotomas, and areas adjacent to these lesions. This type of testing could prove highly useful in clinical settings in order to understand disease progression surrounding areas of vision loss and the effects of particular retinal diseases on the cone photoreceptors.

4.3 Methods

4.3.1 System Design Modifications

Using the real-time eye-tracking software previously described for the TSLO system (Sheehy et al. 2012), a video of the retina was stabilized by actively utilizing the TSLO motion traces for targeted stimulus delivery. Utilizing an acousto-optic modulator (AOM), the imaging laser was modulated to place a stimulus decrement (i.e. turning off the laser in order to write a stimulus) or a stimulus increment (i.e. writing the stimulus with a different wavelength of light than the imaging channel) directly onto a targeted retinal location. The newest addition is a stimulus delivery arm of $\lambda = 532$ nm to write incremental stimuli onto the retina, in this case green light. Here, stimulus delivery has the same placement accuracy as previously noted, with the exception of error caused by the transverse chromatic aberration (TCA) between the imaging laser ($\lambda = 840$ nm) and the stimulus laser ($\lambda = 532$). This has been reported as ~ 0.28 arcminutes per degree in the human retina (Thibos, 1987) measured subjectively and on average 0.21 arcminutes per degree measured objectively (Winter et al., 2015).

Solidworks was used to model the opto-mechanical design of the stimulus delivery arm. Figure 4.1 shows the components used to build the cage assembly from Thorlabs. Light was fiber coupled into the cage assembly and then collimated with a 19 mm focal length lens. A mount for ND filters was then inserted after the lens to control for the intensity of the beam entering the system. Next, a 100 mm focal length lens was inserted just prior to two 45° fold mirrors in order to appropriately relay the beam into the existing TSLO system set-up. The two silver-coated fold mirrors allow for fine adjustment of the position and pointing of the entry beam. All system components are off the shelf parts from Thorlabs.

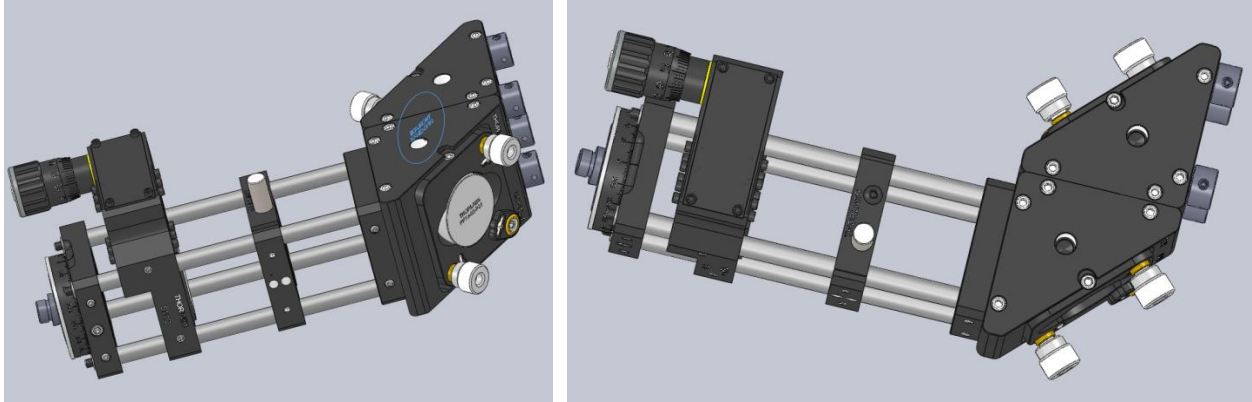


Figure 4.1: Opto-mechanical design of the increment stimulus delivery arm in Solidworks.

4.3.2 Stimulus Delivery Accuracy

To ensure that the targeted stimulus delivery is accurate, a threshold on the cross-correlation peak was implemented. In the current system, whenever the normalized cross-correlation peak is less than 0.3, a decision is made to not deliver the stimulus. Reductions in the cross-correlation peak occur whenever (i) the amount of overlap between the current strip and the reference is reduced (mainly due to horizontal eye movements), (ii) the features within the strip are distorted because of eye motion, (iii) the quality of the image is reduced due to tear film break-up, accommodation, or pupil constriction, (iv) the image is lost due to blinks, (v) the retinal image changes because of lateral and axial pupil displacements relative to the scanning beam, and (vi) there are intrinsic changes in the reflectivity of the retina.

The entire process is computationally demanding and requires a custom solution. In this version, the TSLO data is recorded with a custom-programmed field programmable gate array (FPGA) board (Yang et al., 2010). The FPGA board (Xilinx, San Jose, CA) allows for the immediate access to the strips of image data as they are acquired. The cross correlation with the reference image employs a standard FFT-based algorithm and takes place on a graphics board (Nvidia, Santa Clara, CA) on the host PC. The GPU speed is equivalent to 1GHz, 1600 stream processors with 256-bit interface.

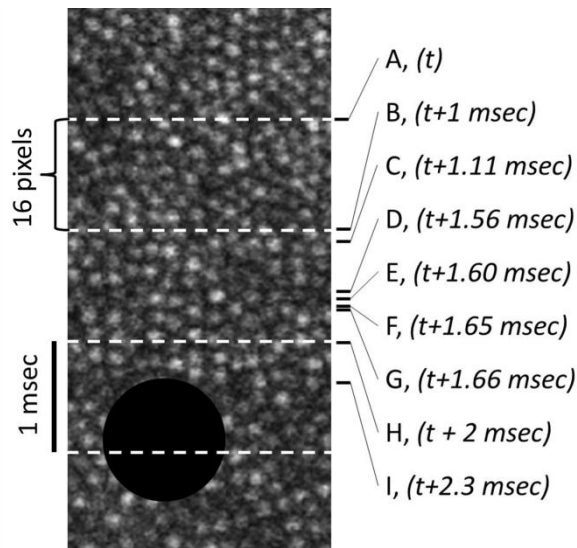


Figure 4.2: Timelines for targeted stimulus delivery. The figure shows a cropped region of an SLO frame split into 16 pixel segments as indicated by the dashed white lines. With a 16 kHz line rate, each 16-pixel segment takes 1 msec to complete as indicated on the right side of the figure. The right indicators show time points for the critical tasks involved in delivering a stimulus, in this case a black circle, to a targeted location. A – Center location of the 32-pixel image strip where position estimate is to be made. B - The final line in the current 32-pixel image strip is scanned and the complete strip is recorded into the FPGA memory. C – The image strip is read into the PC/GPU. D – The eye position at time t relative to the reference frame is estimated by the GPU. E – The time from t to the first line of the buffer that contains the estimated position of the stimulus is computed. F - Make decision: Is there enough time to wait for the next strip before arming the AOM buffer with the stimulus? If YES, then wait for next strip and repeat process. If NO, then proceed to step G. G – Load AOM buffer so it is armed to play out the stimulus while the beam scans over the target. H - Start playing out the AOM buffer at this strip. I - Start delivering the stimulus (note: when the stimulus is greater than 64 pixels in size, steps B to I are repeated for every strip that the stimulus occupies).

The ability to measure eye motion and generate a stabilized video does not directly indicate the accuracy with which a stimulus can be projected onto the retina. While eye motion measurements can be reported at 960 Hz, the delivery of the stimulus involves a prediction and, given the manner in which the stimulus is delivered in the TSLO, some time is required to arm the laser to deliver this. This time is referred to as *latency*. The algorithm is written so that this prediction is completed prior to the beam scanning over the target. Any eye motion that occurs between the prediction and the stimulus delivery results directly in stimulus delivery errors. Therefore, it is important to keep this latency as small as possible.

To compute the latency, fixed frequencies of sinusoidal motion (i.e. 30 Hz) were input into the model eye and the error in stimulus placement was directly observed as relative motion between the dark stimulus and the underlying image. By looking at retinal image strips within the same frame that were recorded prior to the delivery of the stimulus, it is possible to determine the exact location where the motion of the retina was in phase with the stimulus.

This location indicated the time point at which the prediction was made, establishing the latency of the stimulus delivery. The stimulus was observed to move in phase with the retinal locations that were 43 pixels away. Given the actual line scanning frequency of 15.74 kHz, these 43 pixels correspond to a latency of 2.73 msec, which is within the expected range given in figure 4.2.

To measure decrement stimulus delivery performance on a human eye, a black circle of 24 pixels in diameter was used as the stimulus. Multiple videos of the second subject were taken at roughly 600 frames each (except for one video with 300 frames). Figure 4.3 shows a registered sum of 300 stabilized frames from a movie where the stimulus was targeting a retinal location. The sharp stimulus delivery in the average image attests to the tracking accuracy of the system. The video entitled “Stimulus accuracy” in figure 4.4 shows a movie sequence where each frame of the video is cropped around the stimulus. The motion of the retina behind the stimulus is small, but readily apparent. The relative motion between the stimulus and the retinal patch between frames revealed the accuracy of the stimulus delivery (Guizar-Sicairos et al., 2008). Based on 2100 frames from four movies, stimulus delivery failure occurred in 53 frames, or 2.5% of the frames. As described earlier, failures occur whenever the normalized cross-correlation peak of the image strip used to make the prediction of the target location does not exceed 0.3. The frames in which stimulus delivery did not occur were eliminated from motion error calculations. The standard deviation of motion error in the x direction was 0.65 arcminutes and in the y direction was 0.67 arcminutes. This gives an average standard deviation of motion of 0.66 arcminutes, or roughly the size of an individual cone photoreceptor, for stimulus accuracy.

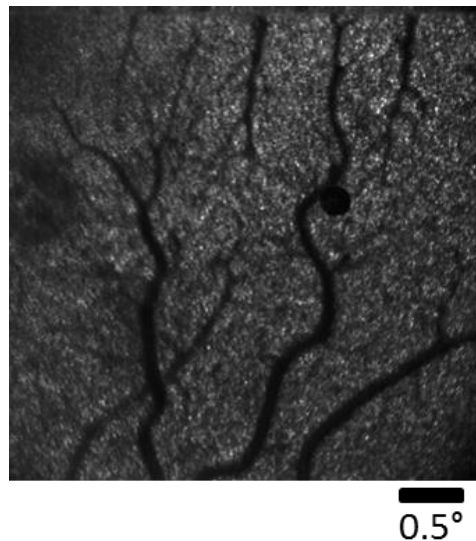


Figure 4.3: Registered sum of 300 frames from a movie sequence where the stimulus was tracking a targeted retinal location.

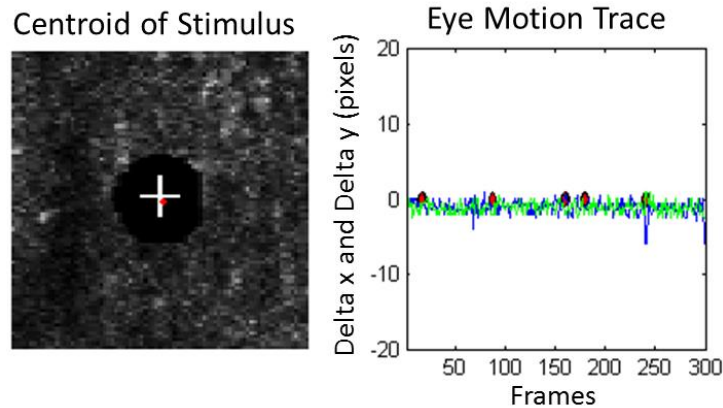


Figure 4.4: Stimulus Accuracy. (Left) A single frame from the 300 frame movie entitled “Stimulus accuracy” showing the centroid of the circle stimulus superimposed upon the retina (Media 1). (Right) Motion error, including microsaccades, for a 300 frame movie. The image of the retina on the left is 30 pixels x 30 pixels. The red diamonds in the graph and media file display the frames in which the stimulus delivery failed.

Increment stimuli placement follows the same latency and accuracy procedure as outlined above, with the exception of the error caused by transverse chromatic aberration (TCA). TCA is the variation of magnification with wavelength and is highly dependent upon the angle of incidence of the incoming beam into the pupil of the eye and the achromatic axis of the eye (Thibos et al., 1990, Simonet & Campbell, 1990). This phenomenon has been previously documented as being a linear relationship – the further the retinal eccentricity, the more TCA is present. For example, using the known conversion of 0.28 arcminutes of TCA offset per degree (Thibos 1987), an eccentricity of 12° would result in a TCA offset of roughly 3.36 arcminutes. Since the TSLO system does not contain an imaging arm for green wavelengths, this level of TCA cannot be corrected for using the image-based methods described by Harmening et al. (2012) and needs to be accounted for when determining exact placement of the stimuli and overall structure/function relationships. In order to minimize TCA errors in the periphery, each subject was asked to foveate at the center of the imaging raster and was aligned for the optimal image at 840 nm by the experimenter. The subject was then asked to manually adjust the position of the green imaging raster to directly overlap with the IR raster at the fovea. This would allow simultaneous optimal IR images with the minimal TCA offset. During offline analysis, any additional TCA accrued in the periphery could be appropriately calculated. Additionally, TCA could also be minimized when the pupil is centered on the optical axis of the eye. In the future, careful attention should be paid to the position of the beam incident on the pupil through the use of a pupil camera when possible.

4.4 Results

Human eye patient data are reported here for two subjects with retinal pathologies, one having toxoplasmosis scarring and the other having an unknown subclinical cause of retinal pathology. Both patients were male and ages 30 and 48, respectively. The experiment was approved by the University of California, Berkeley, Committee for the Protection of Human

Subjects and all protocols adhered to the tenets of the Declaration of Helsinki. Patients were given 1% Tropicamide to prevent accommodation during the experiment. All measurements were recorded with a 5° FOV (512 x 512 pixels) providing a sampling resolution of 0.97 minutes per pixel. The power of the 840 nm light source never exceeded 450 μ W at the pupil plane, which was computed to be well within the ANSI safety limits (ANSI, 2014). A chin rest with temple pads was used to minimize head motion for all human eye experiments.

4.4.1 Patient 1 (P1) Imaging with Functional Testing

Retinal Imaging for patient 1 was performed on the TSLO system using 840 nm light. The patient was instructed to fixate on a target displayed within the 5° imaging raster in order to center the subclinical lesion within the field. The lesion, or area of diminished retinal reflectivity, was located roughly 2.5° inferior of the fovea as seen in Figure 4.5. Traditional fundus photography used within the clinic does not detect this area of minor retinal pathology, thus the ROI was deemed as an area with an “unknown subclinical lesion.” Five locations (shown as small red boxes in Figure 4.5) were chosen in order to test visual sensitivity, both within and surrounding the lesion, using the increment stimuli method explained earlier in this chapter ($\lambda=532$ nm). Through the use of AOMs, modulation of both the stimulus and imaging channels were achieved. By increasing or decreasing voltage values, the AOM functions as an optical switch (turning on and off the laser at different scanning locations within the raster) sending more or less light through, respectively. Due to the fact that the voltage response curve of the AOM is not linear, a look up table was generated in order to calibrate system luminance. Unfortunately, because of first-order scattering from the AOM, there will always be a “leak” present, and this will contribute to the overall luminance of the background. This leak was measured to be 1.14 nW.

Additional structural imaging was performed using a combination TSLO-Bioptigen OCT system. Eye motion traces from the TSLO were sent directly into the OCT system in order to actively steer the imaging beam to stay on target. Further explanation and insight into this active eye-tracking process is discussed in Chapter 5, section 5.6. Figure 4.5 shows the OCT image with the corresponding TSLO image montage for P1. The green vertical line seen on the TSLO image represents the vertical scan taken with the OCT system. All horizontal lines were used to align vasculature between the two imaging modalities. OCT images show the photoreceptor layer slightly elevated, but still intact, going through the lesion.

For the experiment, a 6-pixel green square stimulus (~ 3.5 arcminutes) was flashed for three frames at a 30 Hz frame rate. A 6-pixel stimulus size was chosen because this was the smallest size that could be accurately delivered to the area of interest. Stimuli were stabilized on the retina, using the real-time image stabilization software that corrects for fixational eye motion (Arathorn et al., 2007, Yang et al., 2010). The patient was instructed to respond whether or not they saw the stimulus delivered using arrows on a keyboard (right arrow means they saw the flash, left arrow means they never saw it). Threshold intensity values were measured using a 40-trial QUEST staircase with a yes/no response paradigm. QUEST is an adaptive staircase procedure that estimates the psychometric function between each trial, and

suggests a stimulus intensity that is near threshold. This provides for a better estimate of threshold after fewer trials (Watson & Pelli, 1983). Each chosen location was tested 3 times.

Figure 4.6 shows the threshold intensity values for the 5 locations tested. Light intensity is expressed in arbitrary units – meaning a level of 0 corresponds to the stimulus containing the light of that equal to the background field and a level of 1 corresponds to the maximum power value of the stimulus output from the AOM + the background imaging raster. For this experiment, a level of 1 measured to be $0.065 \mu\text{W}$. Figure 4.6 shows threshold values appear to be very close, or within the standard error of one another, for four of the five locations tested. Location 3, which is located at the center-most area of the subclinical lesion, did result in an elevated threshold compared to the other locations, but not enough to be statistically significant from all other values. Therefore, the subclinical lesion shows no immediate signs of functional loss in this area of lower retinal reflectivity.

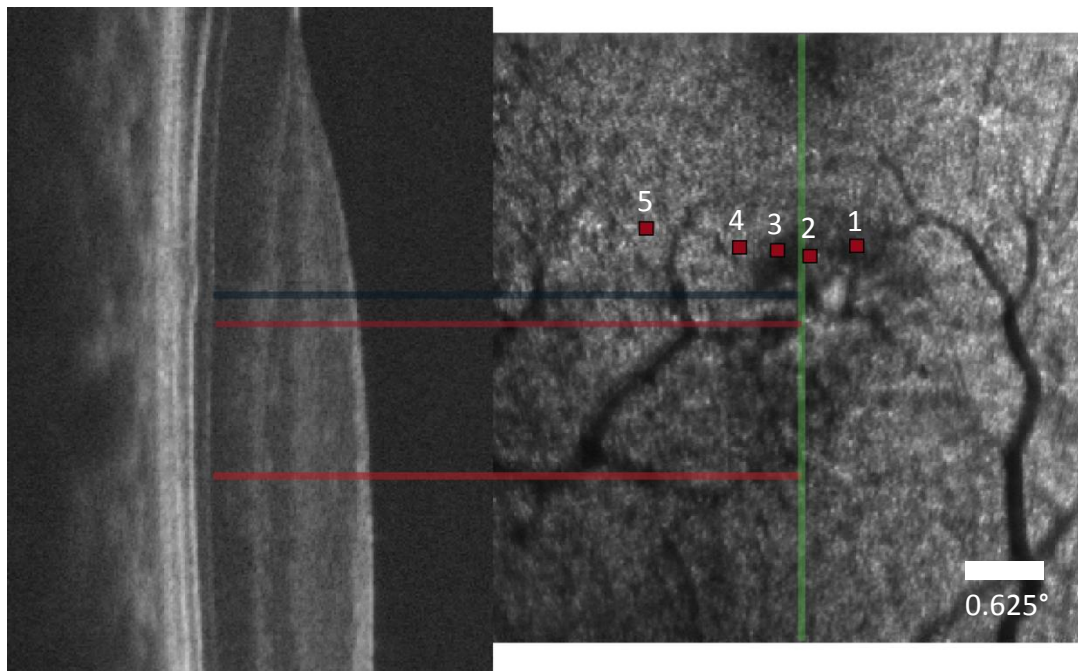


Figure 4.5: Structural montage of the subclinical lesion seen in patient 1. The OCT image is located on the left, with the TSLO image on the right. The fovea is located in the upper center of each image, with the lesion roughly 2.5° inferior. The small red boxes display the actual locations and sizes of the stimulus deliveries (stimulus = 6 pixels). Retinal locations, labeled 1-5, were tested for visual sensitivity 2-4 times each. The green vertical line seen on the TSLO image represents the location of the vertical scan taken with the OCT system. The maroon horizontal lines were used to align vasculature between the two imaging modalities, while the blue line shows where the lesion lines up on both images. The OCT scan shows the photoreceptor layer slightly elevated, but still intact, going through the lesion. The white scale bar represents 0.625° .

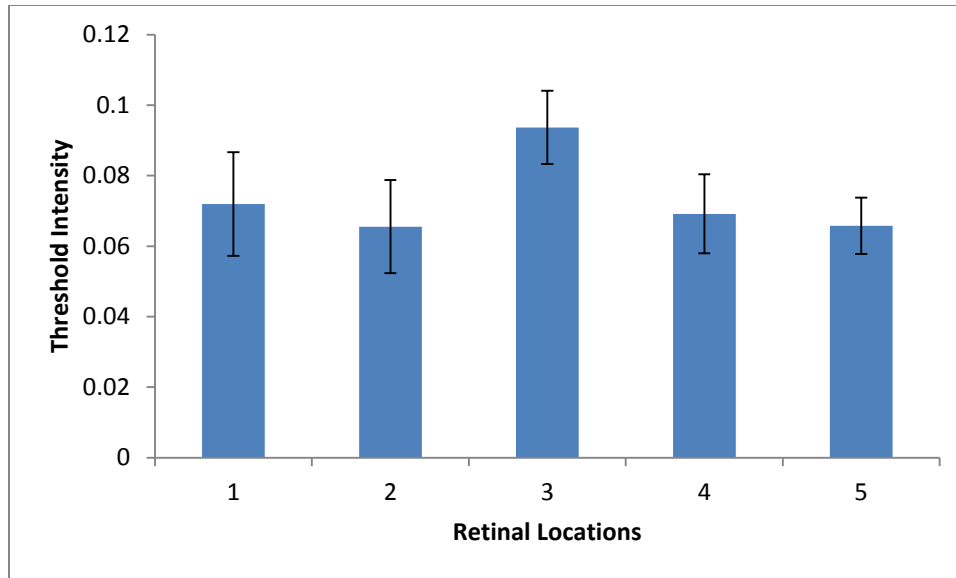


Figure 4.6: Threshold intensity values for all 5 retinal locations tested. Four out of the five locations appear to be roughly the same sensitivity, or within the error, of each other. Location 3, located directly in the center of the subclinical lesion, appears to have a slightly elevated threshold value, but not large enough to be statistically different from all the other locations. Threshold intensity units are expressed in a.u. and error bars represent the standard error.

4.4.2 Patient 2 (P2) Imaging with Functional Testing

Structural imaging and functional testing with the TSLO system were performed on a patient with toxoplasmosis scarring. Toxoplasmosis is a disease that results from the infection of the parasite *Toxoplasma gondii*. Within the retina, the disease can manifest itself as significant inflammation with subsequent scarring. These scars can impair vision and potentially leave scotomas, or blind spots. Toxoplasmosis can most typically be acquired through the organism found in cat feces and is one of the most common causes of inflammation in the back of the eye.

P2 was found to have two clear toxoplasmosis scars, stacked vertically, and located at roughly 12.5° nasal, 10° superior. Two days of imaging/functional testing were completed on the larger of the two lesions (the upper lesion) and temporal adjacent areas. Figure 4.7 shows all eight locations tested over the course of two testing days. Locations 6 and 7 are located immediately adjacent to the edge of the lesion, with location 8 being present within the lesion. Locations 1-5 were chosen to be a comparison of normal retina. For the experiment, a 10-pixel green square stimulus (~ 6 arcminutes) was flashed for three frames at a 30 Hz frame rate. A 10-pixel stimulus size was chosen for this patient experimentally – it was the smallest stimulus size that could be seen in normal regions at the corresponding peripheral eccentricity roughly half of the time. Following the same procedure as for patient 1, stimuli were stabilized on the retina, using the real-time image stabilization software that corrects for fixational eye motion (Arathorn et al., 2007, Yang et al., 2010). Patient 2 was instructed to respond whether or not

they saw the stimulus delivered using arrows on a keyboard (right arrow means they saw the flash, left arrow means they never saw it). Threshold intensity values were measured using a 40-trial QUEST staircase with a yes/no response paradigm and each location was measured 2-4 times.

Additional structural imaging was performed using a combination TSLO-Bioptigen OCT system. Motion traces from the TSLO were actively fed into the OCT system to steer the imaging beam to stay on target. Further explanation and insight into this active eye-tracking process is discussed in Chapter 5, section 5.6. Figure 4.7 shows the OCT image aligned with the corresponding TSLO image montage. The horizontal green line through the SLO image shows where the slice was taken for the OCT scan, with the other vertical lines (maroon and blue) align the two imaging modalities via blood vessels. Clear dropout of the photoreceptor layer is observed in the area directly corresponding to the toxoplasmosis lesion on the right hand side of both images.

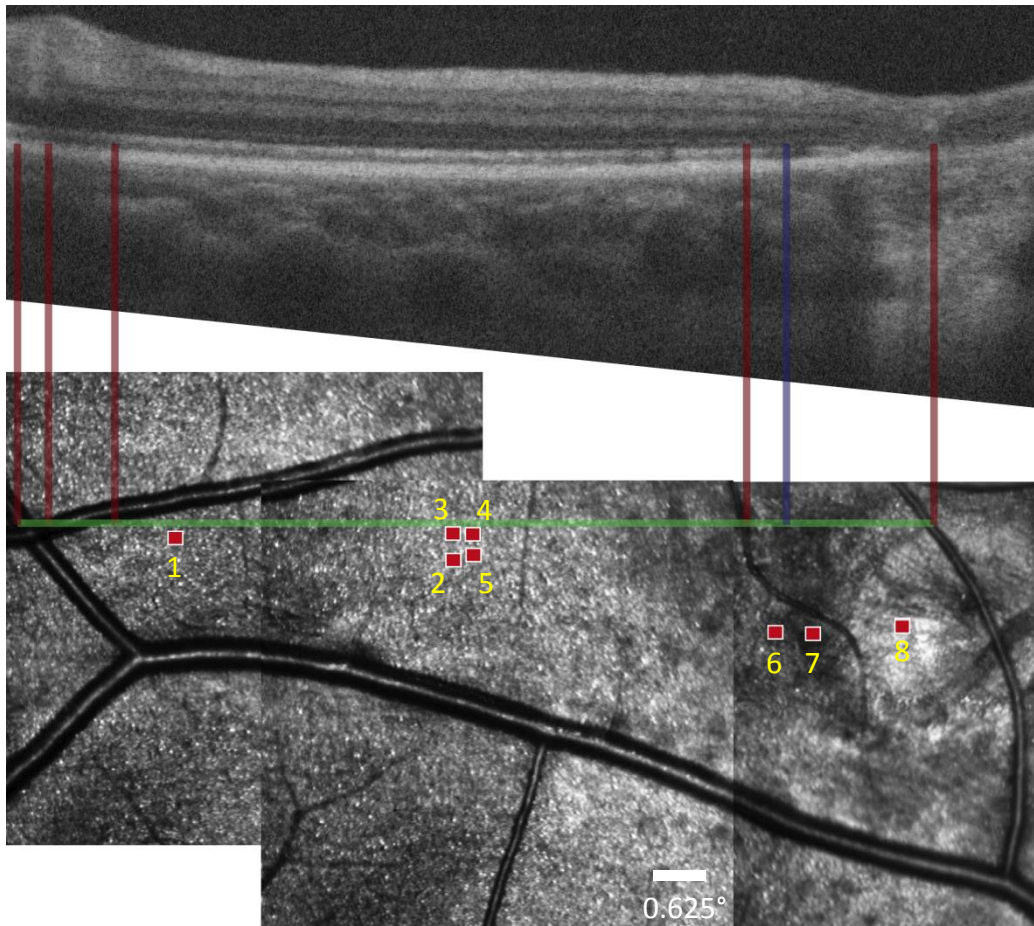


Figure 4.7: Locations 1-8 of functional testing for patient 2 overlaid on the corresponding retinal images (SLO image below, OCT image on top). The red boxes are the actual locations and sizes of stimulus deliveries (stimulus = 10 pixels). Each location was tested 2-4 times each. The green line on the SLO image corresponds to the location of the horizontal scan taken with the OCT system. The maroon vertical lines are drawn for reference/alignment of the blood vessels between images.

The vertical blue line corresponds to the borderline area just outside of the lesion, showing a clear loss in photoreceptor reflectivity in the OCT image. The white scale bar represents 0.625° .

Figure 4.8 shows the eight threshold intensity results for P2 for both testing days. Once again, threshold intensity is plotted in a.u. and varies between 0 and 1. For this experiment, the AOM leak was measured to be 2 nW, with a maximum power + background of imaging raster (a threshold of 1) equaling $0.055 \mu\text{W}$. Locations 7 and 8 were tested to be an absolute scotoma, i.e. the patient never reported seeing the stimulus delivered. Location 6, slightly further away from the lesion, had a slightly elevated threshold response compared to normal threshold intensities, which are the values seen at locations 1 and 5, but was still visible. However, location 2, which appeared to be an area with unaffected retinal structure, also reported an absolute scotoma, with locations 3 and 4 reporting elevated thresholds. This result was unexpected, as the TSLO image gave no indication of any compromised structure. When we compared the TSLO functional imaging locations with OCT structural data, there appear to be no abnormalities located within the photoreceptor or nerve fiber layers for locations 2-4. Further functional testing and structural imaging are required to elucidate this phenomenon.

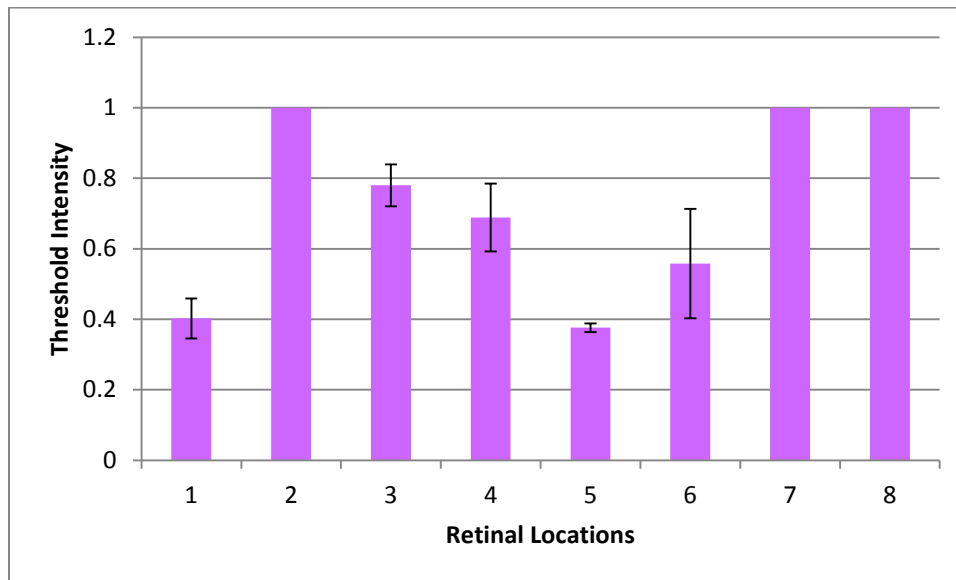


Figure 4.8: Threshold intensity values for all eight retinal locations tested. Three out of the eight locations tested as absolute scotomas (Locations 2, 7 and 8). Locations 3, 4, and 6 appear to have elevated threshold values, while normal threshold intensities were reported for locations 1 and 5. Threshold intensity units are expressed in a.u. and error bars represent the standard error.

4.5 Discussion

Adding the additional light delivery arm for green light allowed for the functional testing of two patients using the incremental threshold technique at targeted locations on the retina.

Areas located within and immediately adjacent to the toxoplasmosis lesion/scar showed no function, or complete visual scotomas, with patchy functional performance up to 5° temporal to the lesion. Elevated thresholds were reported, as well as one area of absolute scotoma in an area that appeared to be structurally normal in both TSLO and OCT imaging sessions.

Threshold values between P1 and P2 were notably different, with P2's thresholds being roughly one log unit higher than those recorded for P1. It is important to note however, that the regions of retinal testing between the two subjects were located at vastly different eccentricities - 2.5° and 10-12.5°, for P1 and P2 respectively. As stated previously in this chapter, the 6-pixel stimulus size chosen for P1 was the smallest possible size that could be delivered accurately with real-time tracking/stabilization enabled. The 10-pixel stimulus size for P2 was chosen for the peripheral lesions, as it was the smallest stimulus size that was visible roughly 50% of the time for the patient. Therefore, since threshold values naturally increase as a function of eccentricity (Scholtes & Bouman, 1977), the log unit difference in the threshold values recorded here are accounted for. For future experiments, further investigation into the presentation of smaller stimulus sizes at the fovea and regions surrounding it for more evenly comparable threshold intensity values should be done.

Due to the fact that this TSLO microperimetry system does not have a green wavelength image capture arm (or PMT channel), TCA in the periphery cannot be compensated for (Harmening et al., 2012). This means that the shift in the green stimuli compared to the IR imaging raster will play a role in the placement of the targeted stimulus delivery. For the locations analyzed in the latter toxoplasmosis experiment, at roughly 10-15° retinal eccentricity, a shift in the green stimulus channel is expected due to TCA to range from about 2.8 – 4.2 arcminutes. For reference, a peripheral cone size is roughly ~ 7 μm (or 1.4 arcminutes) in size (Curcio et al., 1990). This amount of correction or compensation though, assumes that the pupil remains centered on the imaging beam.

Aside from the predicted shift in TCA, pupil position plays a key role in stimulus placement and delivery errors as previously mentioned in this chapter. If the imaging beam is not centered on a subject's pupil, unknown amounts of additional TCA could be present causing a further shift in the targeted stimulus placement. One way to combat this in future experiments would be the addition of a pupil camera to use during image acquisition. This way the experimenter can monitor image quality and position simultaneously, and have immediate feedback on those trials that may need to be discarded/re-done. Since there was no pupil camera present during the course of the aforementioned experiments, the exact location of the beam entering the pupil was not continuously monitored. While careful consideration was made to maximize the IR image quality at all times for minimal TCA, there were no direct measurements of pupil position.

Apart from the aforementioned limitations, the combination of the TSLO microperimetry and imaging capabilities allows for a direct measure of both retinal structure and function. This would allow clinicians to better understand the relationship between retinal

structure and function in diseases, as well as give scientists the opportunity to study fundamental questions of vision/function at the cellular scale.

4.6 Summary

The TSLO was able to provide information regarding both structure and function in two patients with focal retinal lesions. This multi-functional system could be useful in clinical settings to better understand disease progression and the effects of particular retinal diseases on the cone photoreceptors.

4.7 Acknowledgements

This research was supported by grants from the Macula Vision Research Foundation (AR, CKS), the University of California, Berkeley Vision Science Graduate Student Training Grant T32EY007043 (EB) and the National Institutes of Health EY014735 and EY023591 (AR, AB). The author would like to especially thank Ally Boehm for her helpful suggestions regarding experimental protocol, as well as tirelessly imaging the author's retina, and Ethan Bensinger for assistance in extra after-hours imaging/functional testing sessions to fully complete this data set for thesis submission. Additionally, a big thank you to William Tuten for his perimetry code which was adapted for the TSLO system.

CHAPTER 5: The Usage of the TSLO as an External Eye-tracker

5.1 Abstract

This chapter describes a system that combines a tracking scanning laser ophthalmoscope (TSLO) and an adaptive optics scanning laser ophthalmoscope (AOSLO) system resulting in both optical (hardware) and digital (software) eye-tracking capabilities. The hybrid system employs the TSLO for active eye-tracking at a rate up to 960 Hz for real-time stabilization of the AOSLO system. AOSLO videos with active eye-tracking signals showed, at most, an amplitude of motion of 0.20 arcminutes for horizontal motion and 0.14 arcminutes for vertical motion. Subsequent real-time digital stabilization limited residual motion to an average of only 0.06 arcminutes (a 95% reduction). By correcting for high amplitude, low frequency drifts of the eye, the active TSLO eye-tracking system enabled the AOSLO system to capture high-resolution retinal images over a larger range of motion than previously possible with just the AOSLO imaging system alone.

5.2 Introduction

Adaptive optics (AO) imaging systems allow for the visualization of individual photoreceptors in the living human eye (Liang et al., 1997). This technology, when combined with a scanning laser ophthalmoscope (AOSLO), is capable of recording high-resolution movies of the retina in real-time (Roorda et al., 2002). Recent advances in the design of AOSLO systems

have showcased the resolution capabilities of the system by resolving both foveal cones and rods in the human retina (Dubra and Sulai, 2011, Dubra et al., 2011). Apart from its imaging capabilities, the AOSLO system has the capacity to stimulate single cone photoreceptors for microperimetry (Harmening et al., 2014, Tuten et al., 2012, Sincich et al., 2009), and monitor retinal disease progression and treatment over time (Williams, 2011). While the uses of the AOSLO for these tasks are becoming more prevalent in both basic research and the clinic, one major disadvantage remains when using a system at such a fine scale: eye motion.

Online tracking achieved through the recording of eye motion from an AOSLO video alone (Arathorn et al., 2007) has been previously effective for anesthetized monkeys (Sincich et al., 2009) and trained psychophysical observers with normal vision (Harmening et al., 2014, Tuten et al., 2012). However, only one publication reports the use of online tracking for targeted visual function testing in patients with eye disease (Wang et al., 2015). The particular patients in that study had normal visual acuity and fixation. However, many subjects with retinal diseases, particularly those affecting the macula, demonstrate compromised fixational stability (Martinez-Conde et al., 2006) and exhibit larger fixational eye movements than normal subjects (Kumar and Chung, 2014). Compromised fixation in patients may include one or more of the following abnormal eye movements: fixation nystagmus, slow re-fixation saccades, saccadic intrusions and oscillations, superior oblique myokymia, ocular paralysis, or an increased drift or scarcity of microsaccades in amblyopia (Leigh and Zee, 2006). Patients with retinal diseases, particularly AMD, typically have a larger range of fixation than normal subjects, with an average mean motion of just over 4° in the horizontal direction and 3° in the vertical (Kumar and Chung, 2014), as compared to a 0.3° average extent of fixational motion in normal subjects (Cherici et al., 2012).

To enable reliable high-resolution imaging of patients and to make the tracking system more robust for a smaller field of view in healthy eyes, a hybrid tracking scanning laser ophthalmoscope (TSLO) and AOSLO system was built and quantified. Such a system is capable of both optical and digital eye-tracking. Furthermore, the system acts similarly to a woofer-tweeter eye-tracking system; utilizing both software (digital tracking) and an active tilt/tip mirror (optical tracking) in order to achieve real-time image stabilization and correction. It has been shown in previous work with the TSLO system that the allowable eye motion/velocity threshold for digital tracking scales linearly with a system's field size (Sheehy et al., 2012). Therefore, using an external tracking system with a larger field of view (FOV) to guide/steer the AOSLO imaging beam allows for more eye motion to be captured than with the AOSLO system alone. For example, an AOSLO system with a FOV of 0.75° corresponds to an eye motion velocity threshold of $2.6^\circ/\text{s}$, whereas a larger 3.5° TSLO FOV corresponds to a larger range of motion – up to $12^\circ/\text{s}$. Previously, if the fixational extent of motion was larger than roughly 50% of the AOSLO field size, digital tracking would fail. This is no longer a constraint with a larger FOV external eye-tracker.

Previous work has been published regarding the use of eye-trackers with AOSLO systems. Stevenson and Roorda compared a dual Purkinje image eye-tracker (Stevenson and Roorda, 2005) with an AOSLO system to study the frequency contribution of fixational eye

motion at a fine scale. Burns et al. (2007) described the use of a closed-loop tracker that used a dithering probe beam and servo tracking system to lock onto a bright retinal feature. That system was integrated with an AOSLO system and they reported a bandwidth of eye-tracking up to ~ 1 KHz (Burns et al., 2007, Ferguson et al., 2010, Hammer et al., 2006). Yang et al. (2014) described the use of a tip/tilt mirror for active closed-loop eye-tracking with an AOSLO over a 1.5° field of view (FOV). Additionally, eye-trackers have been added to OCT (Vienola et al., 2012, Braaf et al., 2013, Ferguson et al., 2004, Hammer et al., 2005) and AO-OCT systems (Kocaoglu et al., 2014) in both clinical and basic research domains, some utilizing the same TSLO technology described herein. Particularly, the eye-tracker used by both Vienola et al. (2012) and Braaf et al. (2013) was a TSLO system designed and built in our lab. Most recently, Kocaoglu et al. (2014) used hardware based eye-tracking to limit image distortion and blur in AO-OCT images. These experiments and set-ups highlight the current state of the art eye-tracking for high-resolution imaging modalities. The TSLO-AOSLO system combines many of the advantages of prior technologies into one system, such as larger field of view and higher accuracy, into a novel woofer-tweeter eye-tracking system set-up with AOSLO.

The system described herein uses both software and active hardware to achieve real-time, open-loop, high-resolution retinal eye-tracking capabilities. It is the first time a confocal-SLO imaging system has been used to record eye motion and actively steer an AOSLO system to correct for eye motion. This system takes advantage of the fine digital eye-tracking for imaging over smaller fields and for subjects with larger amounts of eye motion. With the tracking accuracy of better than a single foveal cone photoreceptor, the TSLO-AOSLO combination system captures high-resolution retinal images over a larger range of eye motion than previously possible with the AOSLO imaging system alone.

5.3 Methods

5.3.1 Optical Design of an AOSLO System for External Eye-tracking

In order for an AOSLO to perform optical tracking, it needs an active optical element that can move according to the TSLO's motion trace to keep the imaging beam on target. This configuration can be achieved in various ways, but this chapter will discuss the following two methods: (1) using an additional galvo scanner solely dedicated to eye-tracking (with an added telescope to maintain pupil conjugacy) or (2) a piezo-actuated tip/tilt mirror ((Physik Instrumente (PI), Germany) that performs the duties of both the vertical scanner of the system and acts as the active eye-tracking element. Through experimentation, the former of these appears to be a better solution and was implemented in the AOSLO active eye-tracking system built in Bonn, Germany. Figure 5.1 shows the front-end optical design of such a system. Scanning elements and the deformable mirror are placed in the pupil planes of the system. The resonant scanner is placed at the first pupil plane within the beam path, followed by the galvo scanner dedicated to vertical scanning, then the galvo scanner for active eye-tracking, and finally the deformable mirror at the pupil plane closest to the eye. An out of plane optical design was chosen to minimize system aberrations, namely astigmatism, and provide a stable pivot point for the beam at the pupil plane (Gomez-Vieyra et al., 2009). The system employs the

use of two 1-inch mirrors and eight 2-inch ones in order to compensate for the scan field, as well as fixational eye motion. However, during patient imaging or with untrained subjects, eye motion could be larger than the diameter of these 2-inch mirrors causing system vignetting. Therefore, it is important to not only buy an active optical scanning element that can properly steer the beam during all fixational deviations, but to also use optical mirrors/lenses that have a large enough surface to encompass this motion.

The latter sections of this chapter will explain the pros and cons of using the PI piezo tip/tilt mirror approach for active eye-tracking in an AOSLO system that was externally driven according to TSLO eye motion traces.

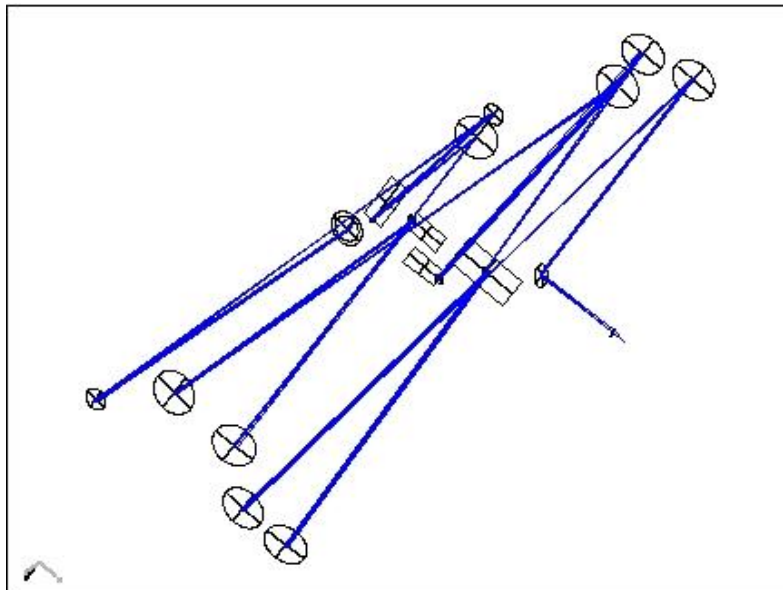


Figure 5.1: Zemax design of active eye-tracking AOSLO system.

5.3.2 Combination of TSLO and AOSLO Systems

The hybrid system is comprised of two modular systems – the TSLO and AOSLO – combined via a notch filter prior to the eye. The 808 nm StopLine single-notch filter was implemented into the system set-up (Semrock, Rochester, NY) which, when used at 45°, allows for nearly 100% of the 730 nm TSLO beam to reflect onto the eye, with the other wavelengths of the AOSLO transmitting through the filter. The TSLO design and set-up have been described in detail in a previous publication (Sheehy et al., 2012). Briefly, a series of three telescopes are used to relay the pupil of the eye onto both horizontal and vertical scanners, with a photomultiplier tube (PMT) used to capture the reflected scanned retinal image. The pupil at the eye for the TSLO system was 3.1 mm. Slight modifications were made to the original system design, including: an off the shelf diode laser (Thorlabs, Newton, NJ), the individual focal lengths of the mirrors, and the replacement of the final spherical mirror with a lens. The lens was used for two reasons: First, having a lens instead of a mirror made the system more flexible in system orientation and allowed for easier coupling into the AOSLO system. Second, the lens

was of a shorter focal length than the mirror prior to it within the final telescope of the system, making a larger FOV for the TSLO than that originally achieved with a system magnification of unity. The system beam magnification and scan angle are inversely proportional (Porter et al., 2006). The field of view is flexible for the TSLO (up to 10°), but was used at 3.5° for these experiments due to the limiting size of the notch filter that was used to combine the two systems. The diffraction-limited optical design and system optimization for the TSLO were completed using optical design software (Radiant ZEMAX LLC, Bellevue, WA). An out-of-plane design, similar to that described by Gomez-Vieyra et al. (2009) and Dubra and Sulai (2011), was used to limit system astigmatism. It is important to note that using an out-of-plane design can affect the rotation of the TSLO imaging raster. System alignment was optimized in order to minimize rotation as much as possible, with subsequent tracking software correction used to account for the remaining rotation. This was done to ensure that any eye motion logged in the TSLO would be sent to the proper axis of the tip/tilt mirror in the AOSLO system for correction.

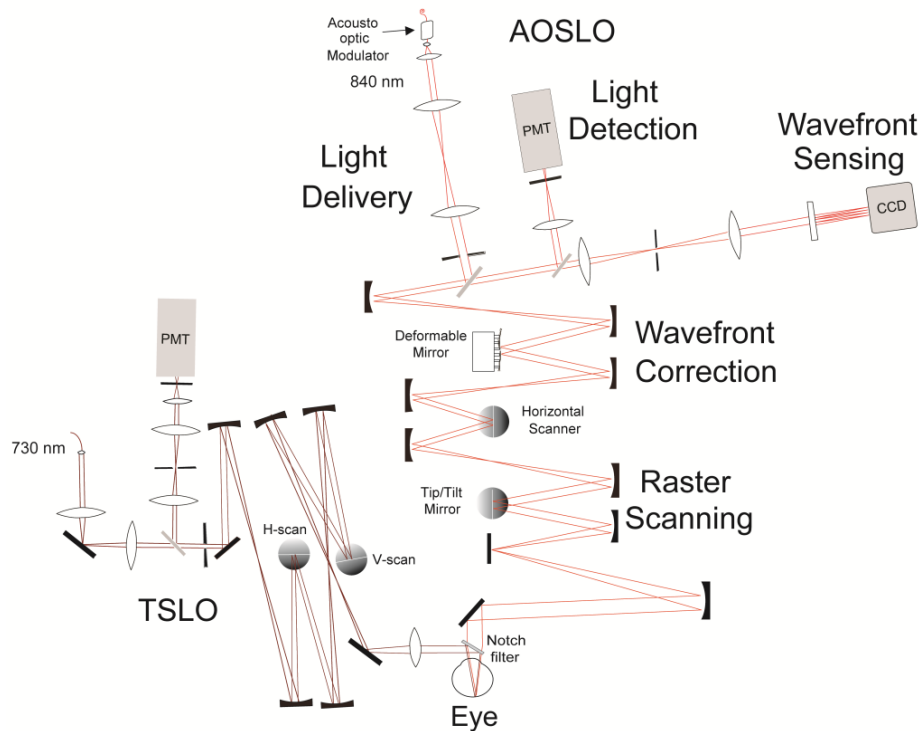


Figure 5.2: A 2-D Optical design schematic of the TSLO-AOSLO combination system. AOSLO: Light exiting the supercontinuum laser is fiber-coupled into the acousto-optic modulator (AOM) before entering the system. The light is collimated and sent through a basic 4f series of lenses onto an adjustable aperture. Light then travels through four mirror based telescope assemblies to the human eye. TSLO: Collimated light exiting the 730 nm laser diode is sent through a 4f system, followed by a 50/50 beamsplitter and then leaves the delivery arm through an adjustable aperture. It travels through a series of three telescopes and joins the AOSLO beam, via the notch filter, into the eye. Light reflected off the retina propagates back through each system into their respective light detection arms. Another series of lenses in a 4f configuration relays the light to be collected at the photomultiplier tubes (PMT). A pinhole is placed at the retinal conjugate planes prior to the PMTs for confocality. The intensity of the signal is sent to two separate PCs for readout (one for

TSLO and one for AOSLO). Note: this is a schematic layout; the actual components are not aligned in a single plane.

The AOSLO experiments described herein used a 0.75° FOV, a smaller field than routinely used for experiments in our lab (1.2° FOV). The AOSLO imaging system itself is almost identical to that reported previously from our lab (Harmening et al., 2012), with the exception of a piezo tip/tilt mirror (Physik Instrumente (PI), Germany) replacing the original galvanometer slow-scanning mirror. The role of the tip/tilt mirror is threefold: (1) to generate the necessary ramp signal needed for the slow scan (30 Hz), (2) to feed the y-motion of the eye in to the piezo, and (3) to feed the x-motion of the eye into the piezo. All motion displacements are sent as voltage signals directly from the TSLO to compensate eye motion. This process will be discussed in more detail in the next section of this manuscript.

5.3.3 Software and Hardware for Open-loop Tracking

The eye-tracking concepts and the software used for digital eye-tracking and reference frame selection for both the TSLO and AOSLO have been reported previously (Arathorn et al., 2007, Sheehy et al., 2012, Yang et al., 2010, and Mulligan, 1997) and so they will only be described briefly here. First, a reference frame is chosen for both systems, typically the first frame to occur during a recorded movie, unless otherwise selected. All subsequent frames are then divided into a series of strips, each of which is cross-correlated with the reference frame. Any translation of the eye from the reference frame is logged as both horizontal (x) and vertical (y) displacements and are measures of the relative motion of the eye at a specific point in time. Both the TSLO and AOSLO data are recorded using a custom-programmed field programmable gate array (FPGA) board (Yang et al., 2010). A standard FFT-based algorithm is used for the reference cross-correlation and is done on a graphics board (Nvidia, Santa Clara, CA) in the host PCs. For the data presented here, 32 overlapping strips per frame are recorded, providing up to a 960 Hz tracking signal from the TSLO (Sheehy et al., 2012).

In order to provide active hardware-based eye-tracking to the AOSLO, the TSLO must send signals to the AOSLO's tip/tilt mirror to compensate for the eye's motion. The optical correction employed here is open-loop. First, the TSLO software tracks the eye's motion over a specified field of view (in the case of this experiment, 3.5°). The eye's displacement in both x and y are logged as motion traces, generating a record of where the eye has moved in real time. Next, the TSLO's motion signal is thresholded via software in order to eliminate noise that could lead to erroneous motion signals sent to the tip/tilt mirror. To do this, eye motion values are monitored over time in order to eliminate spikes that if sent, would result in error. There are two types of thresholding criteria that have been implemented into the system. First, if the active mirror detects a large difference between the currently received pixel position and the previously received one, the new location will not be sent and the tip/tilt mirror will remain at its current position until a new, valid signal is sent. This type of error can occur during a large saccade or blink, causing the pixel differences to be quite large. Experimentally, an "8-pixel" difference was found to be the most appropriate final threshold value for this scenario. Additionally, consecutive "0-pixel" differences can trigger software thresholding. This would

occur in scenarios where the eye has moved and no portions of the image overlap with the reference anymore or if there is a glitch in the software causing an erroneous reading. For up to and including four consecutive “0” values, the mirror will not update its position and will remain at its current position to wait to see if the eye returns to a place that can overlap with the reference. However, if there are greater than four consecutive “0” values, image stabilization is assumed to have been lost by the software entirely and the active-mirror will update to ensure that new image stabilization is enabled. These thresholding constraints occur for both the horizontal and vertical mirror axes simultaneously.

Eye motion is initially recorded in pixel units, which are then converted into two 14-bit voltage signals to be output by the FPGA. To do this, the pixels per degree were measured in the TSLO system using a model eye with a calibrated grid for a retina. Next, varying amplitudes of the DC offset values were input into the PI mirror of the AOSLO system to record how many volts are needed to move one degree (volts/degree). The product of the degrees/pixel in the TSLO and the volts/degree calculated from the AOSLO is the needed voltage/pixel conversion to generate the 14-bit signal for the FPGA. Analog gain amplification was then used to scale the voltage signal sent from the FPGA to match the range of that required by the tip/tilt mirror (Vienola et al., 2012). Due to the fact the tip-tilt mirror is also being used to generate the 30 Hz slow scan signal, a summing junction was used to send the filtered signals to the active mirror in the AOSLO.

The system was set up with a model eye equipped with a galvanometric scanner, to create a “moving retina” to digitally fine tune the conversion parameters until no residual motion was seen in the video of the model eye. The scanner itself was placed between the model eye lens and its retinal plane as seen in Figure 5.3.

In order to better understand the systems’ latencies, the time it takes for the tip tilt mirror to move according to the TSLO motion trace was measured in real time with an oscilloscope. This was found to be 2.5 ms (also reported in Vienola et al., 2012). In terms of digital tracking, any remaining high spatial resolution eye motion artifacts seen in the raw AOSLO video are corrected using the same strip and image based eye-tracking software as that described above for the TSLO system - i.e. the AOSLO system software acquires a reference frame at the beginning of the imaging session in parallel with the TSLO system. It is important to note that this “digital tracking” step is done completely separately in the AOSLO software (Sheehy et al., 2012, Yang et al., 2012).

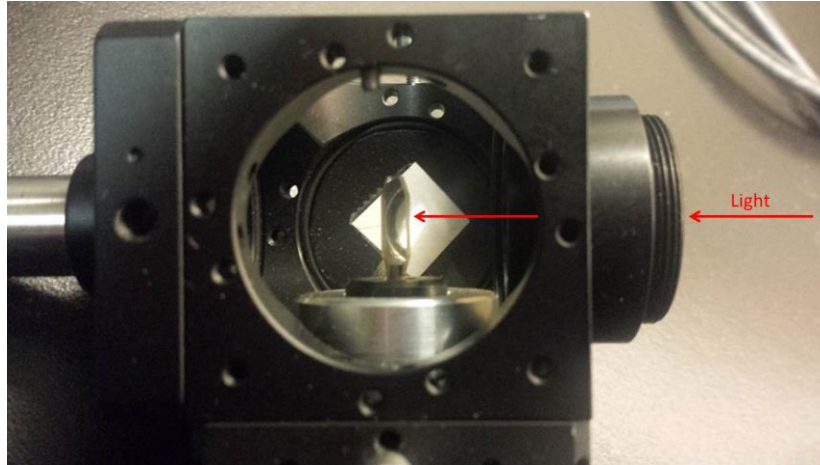


Figure 5.3: Model eye equipped with a galvanometric scanner to create a “moving retina.” Light enters the assembly through a 50 mm focal length lens, hits the silver scanning mirror towards a piece of paper with tape crisscrossed over its center located one focal length away from the lens. The tape offers multiple depths to the “retina” as well as visual landmarks of varying reflectance for the image. Light is then reflected back through the assembly, making it double pass.

5.4 Results

5.4.1 System Bandwidth Analysis for active-tracking with a PI mirror

This experiment was approved by the University of California, Berkeley, Committee for the Protection of Human Subjects. All protocols adhered to the tenets of the Declaration of Helsinki.

The scanning model eye was input into the final pupil plane of the combined TSLO and AOSLO system in order to test the maximum amount of motion that could be successfully imaged in the AOSLO system with active eye-tracking enabled. To do this, varying amounts of frequency and amplitude of a sinusoidal wave were input into the model eye (moving retina) using a waveform generator. Six frequency values, as seen below in Figure 5.4, were chosen and increasing levels of amplitude at each frequency were added until the AOSLO system alone was no longer able to digitally track and stabilize the retinal image. The raw AOSLO videos were then recorded. Next, the same frequency and amplitude values were input into the system with active tracking enabled. Previous values that caused AOSLO stabilization alone to fail could now be tracked using the active tip/tilt mirror to keep the AOSLO imaging beam on target. A raw AOSLO video with only optical tracking enabled was recorded (as well as the previously mentioned raw AOSLO with no tracking) and the residual motion as a function of frequency was subsequently calculated using an offline program that could analyze the videos with the same strip-based analysis, but with higher resolution (Stevenson and Roorda, 2005). The offline program was set to compute eye motion trace at 64 strips per frame, or 1920 Hz. Figure 5.4 shows the percent amplitude reduction with tracking enabled, using a model eye, in the green curve. For lower frequencies, which mainly encompass drift, the optical tracking is able to

sufficiently reduce the amplitude of motion; however, by the time it reaches 10 Hz, the amplitude reduction is down to 65%. Then, the data acquired by our model eye was compared to a computed system bandwidth based on: (1) the bandwidth of the strip-based tracking algorithm in the TSLO (50% amplitude correction at 400Hz (Sheehy et al., 2012)) combined with (2) a measured motion trace latency from the TSLO of 2.5 ms and (3) the frequency response curve of the active tip/tilt tracking mirror (50% drop in amplitude at 80 Hz). The frequency response curve of the tip-tilt mirror was measured experimentally by recording the scanning amplitude response of the mirror to a sine wave input with fixed amplitude as a function of temporal frequency. The overall computed performance is shown as the purple curve in Figure 5.4. For frequencies of 10 Hz, the computed bandwidth is 84%, with a 50% correction cutoff of just over 30 Hz. The experimental bandwidth is slightly lower, possibly, due to the fact that it has to both drive a sawtooth signal as well as track the eye, but compares reasonably well with the expected bandwidth.

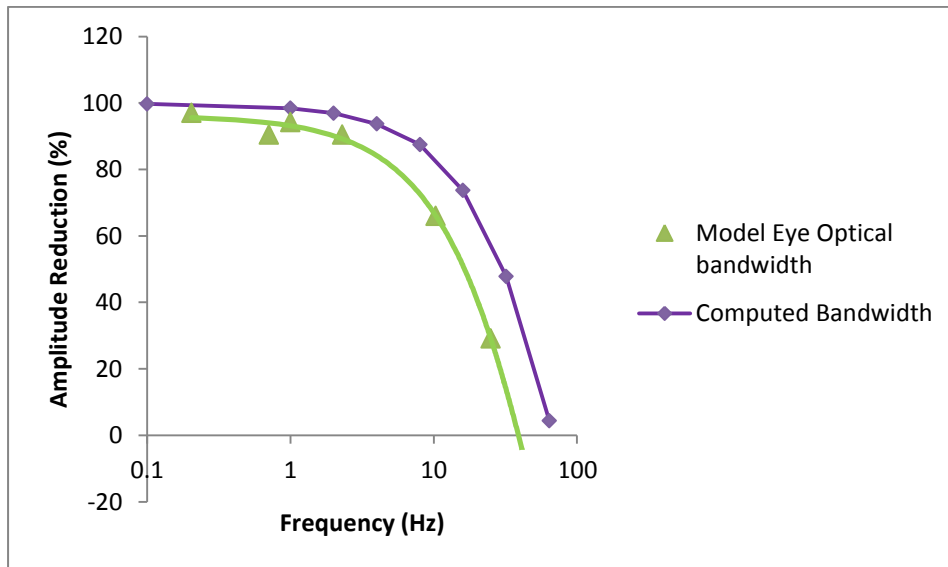


Figure 5.4: Amplitude Reduction (%) vs frequency obtained for both a model eye (measured experimentally and shown in green) and the computed system bandwidth (modeled using TSLO performance with a motion trace latency of 2.5 ms and the tip/tilt mirror’s frequency response curve) is shown in purple.

5.4.2 Human Eye Motion Frequency Analysis

Human eye frequency data are reported here for four normal subjects, between the ages of 26-49, all experienced in AOSLO imaging protocols. A bite bar was used in order to minimize head motion for all human eye experiments.

Subjects were instructed to look at three corners of the 3.5° TSLO raster and were imaged at the same three retinal locations surrounding the fovea – upper left, lower left, and lower right hand corners respectively. (+/- 1.75°). TSLO and AOSLO videos of 300 frames (10

seconds) each were captured simultaneously in order to compare the raw eye motion of the TSLO with the residual eye motion in the resulting AOSLO videos. All images were recorded in conventional fundus view. Figure 5.5 shows the average of a 300 frame AOSLO video overlaid on an average of 300 frames of the TSLO video.

In order to clearly see the percent reduction of eye motion that occurs post eye-tracking, it is important to understand what the different stages of tracking are. A “raw video” refers to a TSLO video which has had no motion correction and contains the actual eye motion of the subject over the imaging session. “Optical tracking” refers to the active tracking or use of the tip/tilt mirror in the AOSLO. The result of optical tracking is seen in a raw AOSLO video, which appears to be mostly stabilized. “Optical + digital tracking” refers to the correction done by both the active tracking of the tip/tilt mirror (optical tracking) and the final stabilization of the AOSLO video using the image-based eye-tracking software (digital tracking). The videos in figure 5.6 show real-time movies of the TSLO (not tracked) and AOSLO (tracked) systems before and after digital and optical tracking, while figures 5.7 and 5.8 show the eye motion traces generated from these videos.

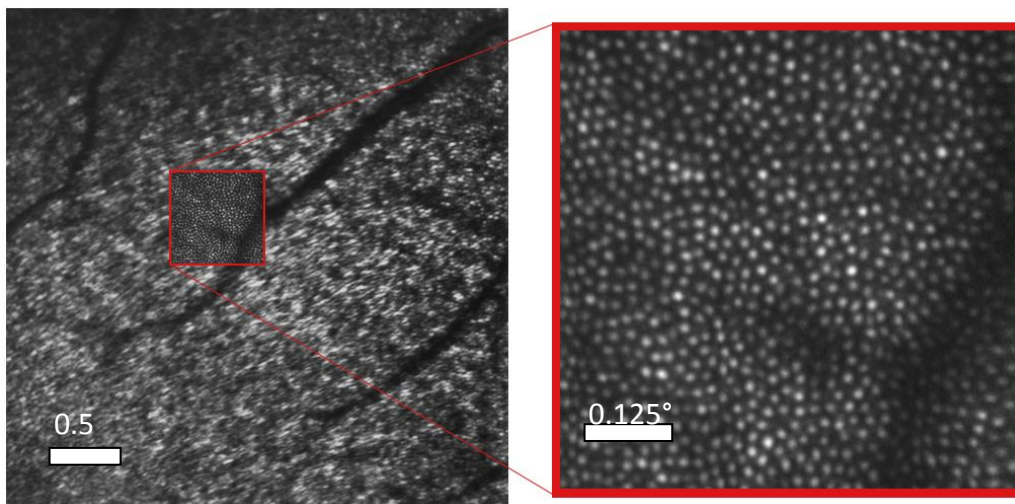


Figure 5.5: TSLO and AOSLO retinal images. The image of the TSLO is shown on the left (the subject is fixated on the corner of the TSLO raster and, in this case, the fovea is on the lower left of the image), with the AOSLO smaller field shown in a red box within it. Note the TSLO image is rich in structure – high contrast blood vessels with cones at larger eccentricities (in the upper right of image) and interference artifacts at lower eccentricities. On the right is the high-resolution AOSLO image where each white spot represents the scattered light from an individual cone photoreceptor. The field of view of the TSLO and AOSLO was 3.5° and 0.75° respectively.

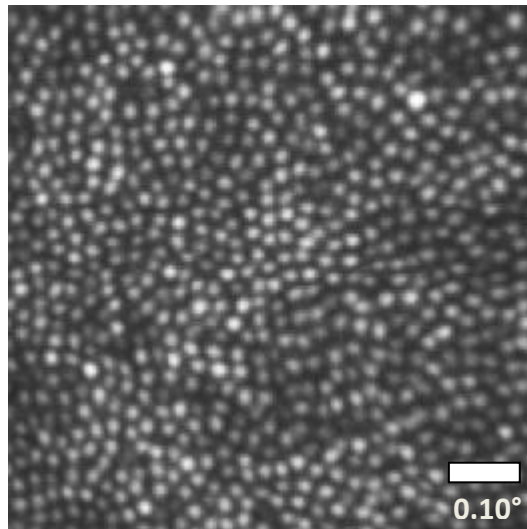


Figure 5.6: Averaged AOSLO video. Image generated from the registered sum of 300 frames from the AOSLO movie with both optical and digital tracking enabled. Note that roughly halfway down the above image, a slight compression is present due to eye motion captured in the reference frame. The steps to obtaining the final image are best shown by a sequence of videos. Media 2 shows the raw 3.5° TSLO video with the natural fixational eye motion. Media 3 shows a stabilized TSLO video after online image based stabilization. The byproduct of the stabilized video in Media 2 is the eye motion trace, which is sent to the tip-tilt mirror in the AOSLO. Media 4 shows the AOSLO video with correction from the TSLO (optical stabilization). The features in the video remain relatively stable, although there are high frequency artifacts present. Media 5 shows the same 0.75° AOSLO video after online digital stabilization. It is cropped to show only the portion of the frame that is not affected by the tip-tilt mirror artifacts. Aside from some frames where the tracking failed, the features remain stable to within a fraction of a cone diameter.

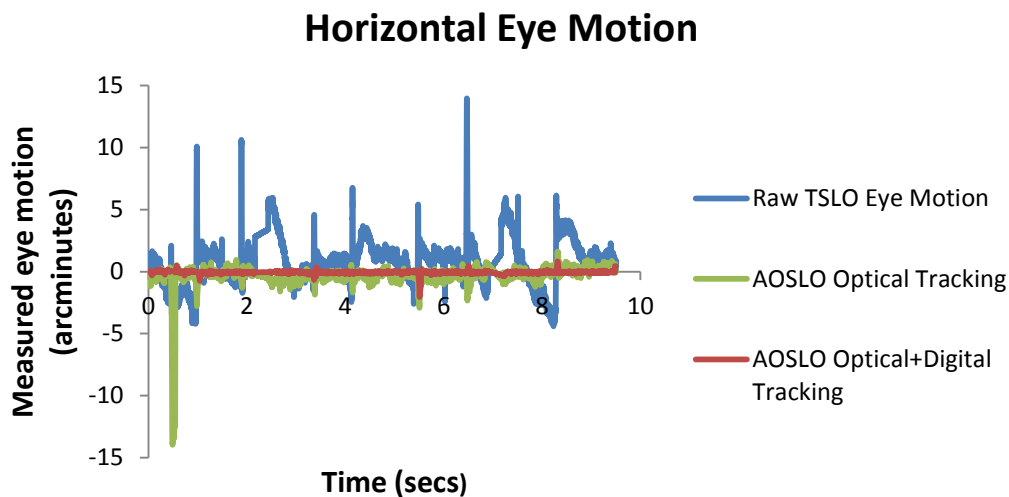


Figure 5.7: Measured horizontal eye motion traces from the above media files. The blue curve depicts the natural fixational eye motion of the subject over the course of the imaging session (as measured in the TSLO system). The large spikes in blue above occur during the microsaccades and

blinks, as seen in the videos. The green curve represents the remaining eye motion after optical tracking was enabled (as measured in the AOSLO system). Finally, the red curve shows the remaining motion with both optical and digital software tracking enabled in the AOSLO system. Any spikes seen in the green or red curve resulted from tracking error.

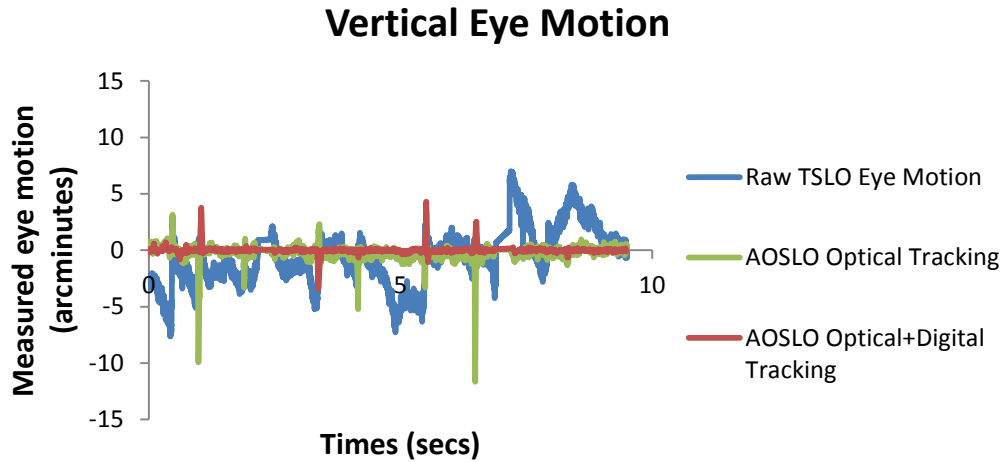


Figure 5.8: Measured vertical eye motion traces from the subject in the provided media files.

Out of the 12 videos recorded at the three locations, 9 of them were analyzed for residual motion using an offline stabilization program set to generate eye motion traces at 64 strips per frame, or 1920 Hz (Stevenson and Roorda, 2005). The subset of videos chosen were those in which 285 or more of the 300 (10 sec) recorded frames were available for analysis (i.e. not containing multiple blinks and/or large saccades that resulted in frame rejection). AOSLO videos were cropped to eliminate mirror response delay at the top of each frame. The eye motion data was then resampled to generate a uniformly sampled time-series at 960 Hz and Fourier-transformed to generate amplitude v.s. frequency spectra. The spectra were calculated for each of the nine videos (so as not to weight one subject or location more than another) and then averaged together to display the overall frequency contributions of the four subjects. Figures 5.9 and 5.10 show the average frequency contribution of the horizontal and vertical motion of the raw eye motion respectively from: the TSLO videos, the residual frequency seen in the raw AOSLO video post optical tracking, and the final frequency spectrum when using both optical and digital eye tracking. The “Optical Tracking” curve shown in blue shows an amplitude of motion of at most 0.2 arcminutes for horizontal motion and 0.14 arcminutes for vertical motion. The “Digital + Optical Tracking” curve shows that the amplitude of eye motion is kept below 0.08 arcminutes for all frequencies in the horizontal motion plot and kept below 0.05 arcminutes in the vertical motion plot. This corresponds to an average amplitude reduction of 95%. The peaks seen at the 30 Hz frame rate and subsequent harmonics are artifacts that arise due to the torsion of the eye as well as distortions in the TSLO and AOSLO reference frames. These artifacts will be explained further in the discussion. Bandwidth estimates were not computed directly from these data since the average spectra from only 9 videos were too noisy to yield sensible results at frequencies above 5 Hz. A basic analysis shows

that the bandwidth is close to, but not as high as, the computed bandwidth or that measured in the model eye.

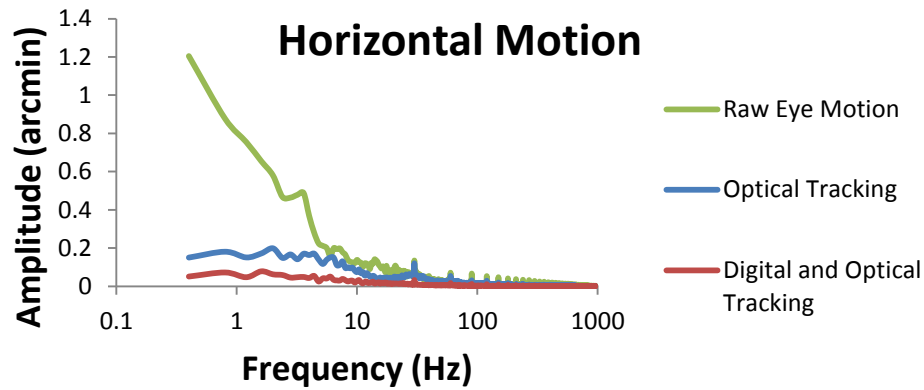


Figure 5.9: The reduction of horizontal eye motion as a function of frequency. Raw eye motion represents the actual eye motion recorded by the TSLO system. Optical tracking refers to the raw AOSLO video, where the tip/tilt mirror was actively correcting for eye motion. Digital and optical tracking represents the active eye tracking plus subsequent software correction. 30 Hz (and subsequent harmonics) reference frame and torsion artifacts are visible in the plot.

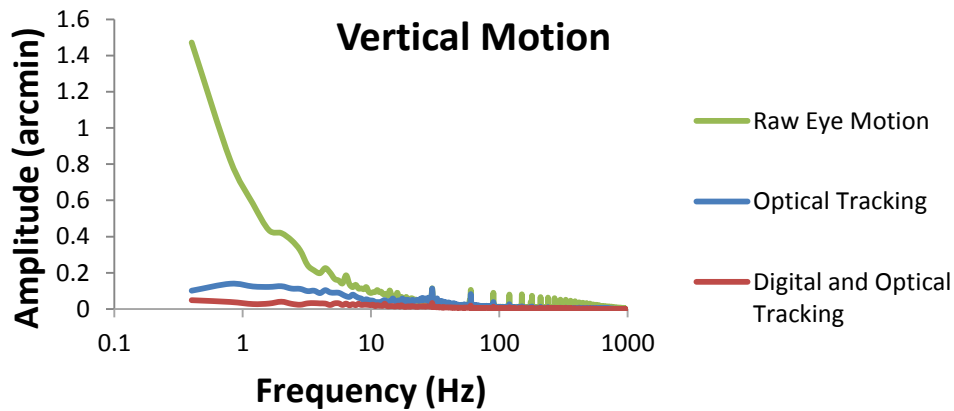


Figure 5.10: The reduction of vertical eye motion as a function of frequency.

5.5 Discussion

The TSLO was combined with the AOSLO system in order to provide real-time optical and digital eye-tracking. Motion traces from the TSLO were sent in the form of voltage signals to the AOSLO tip/tilt mirror in order to compensate eye motion. An average amplitude reduction of 95% was measured in the final stabilized AOSLO videos (optical + digital tracking).

The advantages of using the TSLO for eye-tracking are five-fold:

- 1.) Although the bandwidth of the TSLO is ultimately limited by the motion trace reporting latency of 2.5 ms, the correction is more than sufficient to track the motion of the eye, whose power spectrum of motion falls off with approximately a 1/frequency dependence (Findlay, 1971). The stability of the optically stabilized AOSLO raster makes it better suited for subsequent digital correction of the residual, uncorrected motion.
- 2.) The stability of the optically stabilized AOSLO raster is also expected to yield better adaptive optics corrections since the source of the signal from the wavefront beacon is more stable. This may be especially beneficial in patients with fixational instability using a TSLO system with a larger field of view.
- 3.) By compensating motion artifacts, stimulus delivery to specific retinal locations is expected to be more repeatable and therefore more reliable. This could prove extremely beneficial in patient imaging and vision testing. Many subjects with retinal diseases demonstrate compromised fixation stability, with larger fixational eye movements than normal subjects (Martinez-Conde et al., 2006, Kumar and Chung, 2014).
- 4.) The TSLO offers a flexible and larger field of view than AOSLO systems. This can help operators orient themselves during an imaging session by locating larger retinal landmarks, such as blood vessels or certain cones. A FOV of 3.5° was used in these experiments, but can be easily adjusted to larger field of views by exchanging the final lens of the TSLO system.
- 5.) The TSLO and AOSLO are modular – meaning that they can be used together or separately with the insertion or removal of a filter. This can allow a laboratory to run experiments on both systems – together or separately.

The TSLO system has disadvantages for external eye-tracking as well. Eye motion traces that are sent to the AOSLO are based on the displacements of the eye from a reference frame. Since the retina is scanned over time, each frame in a movie has unique distortions, including the reference frame. The use of a distorted reference frame gives rise to periodic artifacts in the eye motion trace (at the frame rate and at higher harmonics) that are sent to the tip/tilt mirror. However, real-time feedback is provided to the operator if the choice of a reference frame is poor - a warped stabilized image will appear and a new reference frame can be chosen. These artifacts will also be readily apparent in the AOSLO with optical tracking. In fact, since the periodic reference frame artifact from the TSLO and the frame rate of the AOSLO are very close, but not necessarily identical, the distortion often appears as a scrolling distortion in the AOSLO video at the beat frequency between the two frame rates. These reference frame artifacts are visible in the frequency spectrum as peaks at 30 Hz and higher harmonics. It is important to note then, that the frequency contributions of 30, 60, 90 Hz etc. shown in this paper are not solely eye motion contributions and should not be treated as such. Next, whenever the eye makes movements that are orthogonal to the fast scan direction, the TSLO loses its continuous track and the frame acquired after the vertical movements will contain strips that do not overlap with the reference frame (Sheehy et al., 2012). At present, the software holds onto the latest recorded eye position during the blank intervals until new reliable eye-tracking data is

generated. Another disadvantage that must be noted is that TSLO tracking is performed in open-loop. Open-loop tracking requires a one-time initial calibration in order for the larger field TSLO image to scale its output motion traces for the tip/tilt mirror in the AOSLO system. Calibration however, is not required for closed-loop tracking with the same active tip/tilt mirror as described by Yang et al. 2014. Additionally, the extent of eye motion correction has a hard limit based on the size of current system optics. Eye motion that is larger than the maximum FOV that can be accommodated by the AOSLO system optics (in this case, up to 4°) will cause the beam to become vignetted and data to be potentially lost. Lastly, proper alignment of the TSLO and AOSLO pupil planes at the eye are crucial for the high-resolution imaging in both systems simultaneously. It was observed that during the imaging session, if the TSLO alignment became even slightly off, image quality was severely affected.

In the AOSLO system, the active tracking was achieved by a single tip-tilt mirror. To replace the galvanometer of the system with a single element that can provide both the slow scanning capabilities and correct for the eye's motion is certainly a benefit, as the addition of a telescope is not needed for another scanning element. However, there were many difficulties using the tip-tilt mirror for active tracking. Since, the demands of driving the 30 Hz sawtooth may have compromised the bandwidth performance (Figure 5.3); we wanted to perform a more thorough investigation. We monitored the mirror's response on an oscilloscope using the input signal and saw that the linear portion of the ramp signal was sufficient, but there were large "ringing" artifacts after each fly-back of the scanner, which generated significant distortion artifacts at the top of each frame. Electronic tuning of the scanner helped to minimize this substantially, but could not completely eliminate these artifacts. As it stands, the mirror frequency bandwidth is inadequate for a 30 Hz sawtooth ramp signal. For users who are only interested in imaging, this is not an issue, as one can simply remove any extraneous error or delay from the top of the image and use the remaining portion. For tracking applications, however, a continuous eye motion record can be crucial and one cannot simply ignore a portion of the image. Given the limits of today's tip-tilt mirror technology, the use of two galvanometers instead of a single tip/tilt mirror could be a better solution.

5.6 Combination of the TSLO with OCT Systems

5.6.1 Combination of the TSLO with OFDI OCT System

The TSLO can be used as an external eye-tracking system for optical coherence tomography (OCT) systems as well. OCT uses the basic principle of interferometry to measure the reflections of light from different retinal layers within the eye referenced to the reflection from a planar reference mirror. These reflections result in a cross sectional view of the retina, where each layer is delineated by varying intensity values based on the optical path length that light traveled, and can be used in order to calculate various retinal layer thicknesses. Over the last twenty years, OCT systems have added angiography capabilities, allowing the visualization of *in vivo* vasculature of the human eye. To do this, blood flow within the vessels themselves are detected and recorded as phase differences between scans, as described by Braaf et al. in 2011. However, one major limitation of OCT angiography imaging is eye motion. Fixational

instability causes unpredictable motion that can cause an image to look disjointed or anatomically incorrect. This scenario can prove troublesome when such errors result in missing data or false data interpretation.

The TSLO system was combined with the phase-stabilized optical frequency domain (OFDI) imaging system via beamsplitter in Rotterdam, Netherlands. The system uses a 1 μm swept source with a 100 kHz fixed repetition rate and fiber-based interferometer (Braaf et al., 2011). In order to actively stabilize the imaging beam in real time, an active scanning element was implemented prior to the combination beamsplitter (Vienola et al., 2012). Figure 5.11 shows the system set-up; both horizontal and vertical eye motion was compensated for optically. To do this, the motion of the target was fed into the OFDI system in order to actively steer the imaging beam to stay on target.

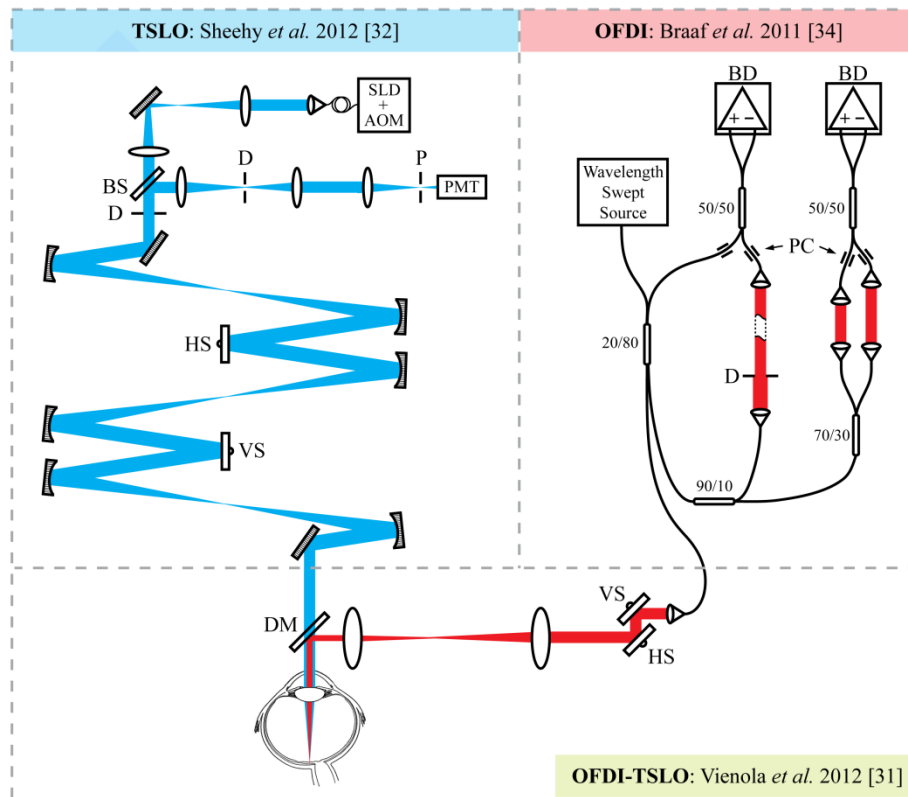


Figure 5.11: The optical layout of the combined OFDI-TSLO setup. (TSLO PANEL) The TSLO schematic with its optical paths in blue. A super luminescent diode (SLD) was used as the light-source combined with an acoustic-optic modulator (AOM). The light is directed via a set of lenses to three curved mirror telescopes to image a horizontal scanner (HS) and a vertical scanner (VS) onto the pupil of the eye. A beam splitter (BS) was used to relay returning light to a photomultiplier tube (PMT) for detection. A pinhole (P) is used to provide confocal retinal imaging and two diaphragms (D) are used to control the input beam size on the eye and to block light scattered within the setup from the PMT. (OFDI PANEL) The OFDI schematic with its optical paths in red. Light from a wavelength swept-source is passed on into a fiber-based interferometer that splits into a sample arm to the eye and a reference arm. Scattered light from the eye is recombined with

the reference arm light at a 50/50 coupler and detected with balanced detection (BD). An additional Mach-Zehnder interferometer was attached to the reference arm with a 90/10 coupler to simultaneously measure a calibration signal and forms the second interferometer channel. Interferometric detection was optimized using in-line polarization controllers (PC). (OFDI-TSLO PANEL) The TSLO and the OFDI were coupled together via a dichroic mirror (DM) (Courtesy of Braaf et al., 2013).

Volume OCT images were acquired in a human subject in order to test the tracking benefits of using a TSLO system. *En face* images were obtained by integrating over depth each B-scan volume set and the corresponding motion traces from TSLO were plotted for comparison. Figure 5.12 shows the same 10.6° retinal scan field both with tracking engaged and without tracking. The images clearly show that fixational motion can distort the resulting vasculature images. To the left of each image is a record of eye motion (green = vertical, blue = horizontal). Abrupt changes/peaks in the motion trace show the occurrence of saccades or blinks, which reveal themselves as distortions and losses of data, respectively. Column (A) shows the ramifications of what can happen to images without tracking enabled, while column (B) shows continuous vasculature with tracking on. If tracking fails however, OCT images are still susceptible to artifacts, as seen in (D).

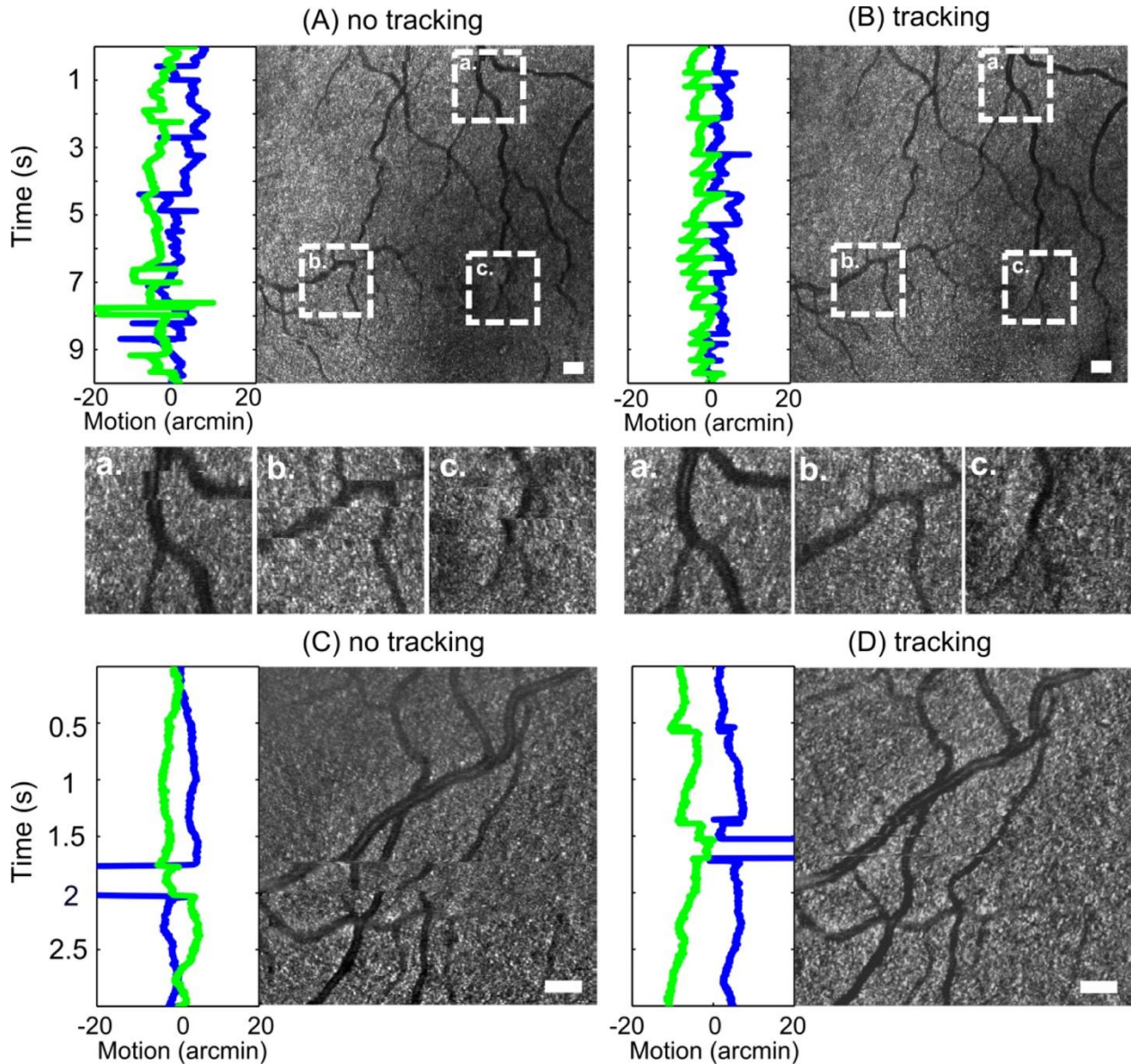


Figure 5.12: En face images from four different volume data sets. (A) Large field of view (10.6° or 3.11×3.11 mm) was imaged without tracking enabled. On the left of the image, the corresponding eye traces are plotted. Below the image, three different areas are shown as zoomed versions from the large image. (B) Same area imaged as in A but tracking was enabled. Enlarged areas show that the motion artifacts are compensated. (C) The smaller field of view (5.3° or 1.56×1.56 mm) clearly demonstrates eye motion artifacts. One large saccade causes the scanning grid to acquire data from different position. (D) Same area imaged as in C but with tracking enabled. In this data set, there is a large saccade that is tracked well. However, the final image still shows artifacts from brief tracking failures. To fully compensate large eye motions, a validity signal needs to be used to rescan the areas that are affected by improper tracking. Scale bars indicate 0.5 deg (Courtesy of Vienola et al., 2012).

The ultimate goal of external tracking is to give artifact-free images of the retina. Therefore, if tracking fails, it is necessary for the TSLO to communicate with the OCT system to

alert the scanners of such an occurrence and require a re-scan of that area to prevent data loss. Figure 5.13 shows what images look like if a validity signal is implemented into the imaging protocol requiring the scanners to remove corrupted B-scans and re-scan the area.

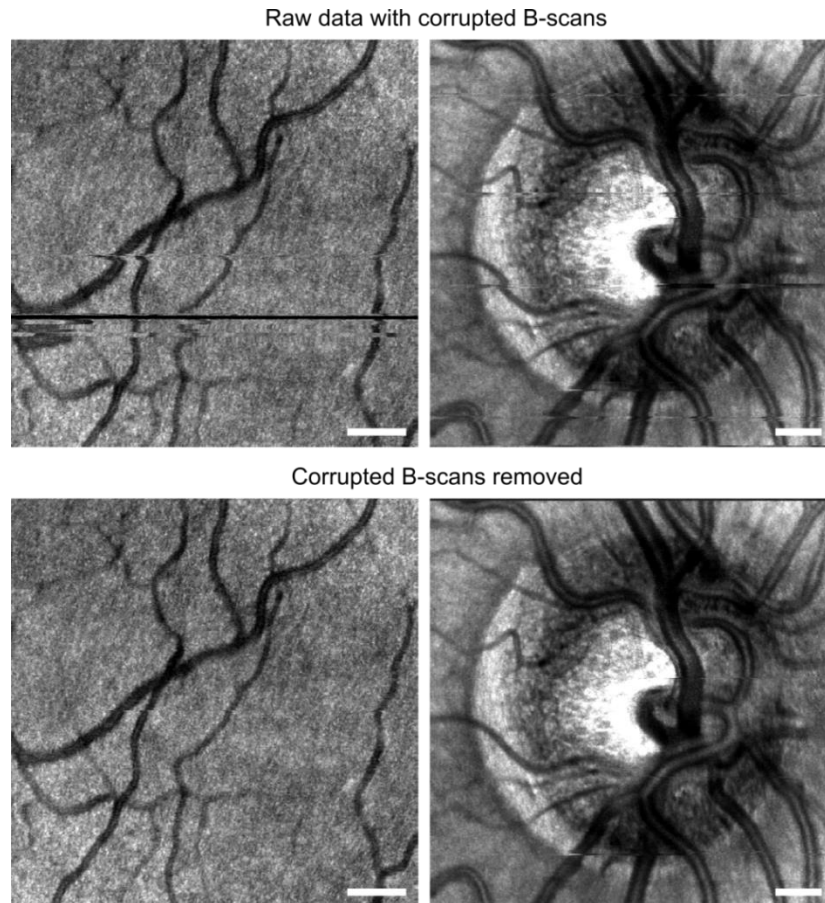


Figure 5.13: Tracked en face images with validity signal. When tracking software lost tracking due to a large saccade or blink, OCT-PC was signaled to step back 10 B-scans and hold that position until tracking was locked again on target. B-scans collected during tracking failure are removed in post-processing and replaced with rescanned counterparts. (Top images) En face of all acquired B-scans is shown. This includes B-scans acquired during large saccades or blinks. The blink is seen as a black line in the upper left image. (Bottom images) Motion or blink corrupted B-scans are removed from the volume data set. The black line caused by the blink is gone and several large saccades are also removed. Scale bars indicate one degree (Courtesy of Vienola et al., 2012).

When mapping vasculature within the retina, artifact-free images are key to quick and accurate image registration. Figure 5.14 showcases 8 volumes compounded to make a high signal to noise image that allows one to see a complete vasculature network. The volumes were acquired using the TSLO-OFDI combination system, with active eye-tracking enabled. A 10 Hz low pass filter was used in order to eliminate noise generated from reference frame artifacts. Additionally, a validity signal was used in order to remove frames that occurred during blinks or large saccades and to re-scan said areas.

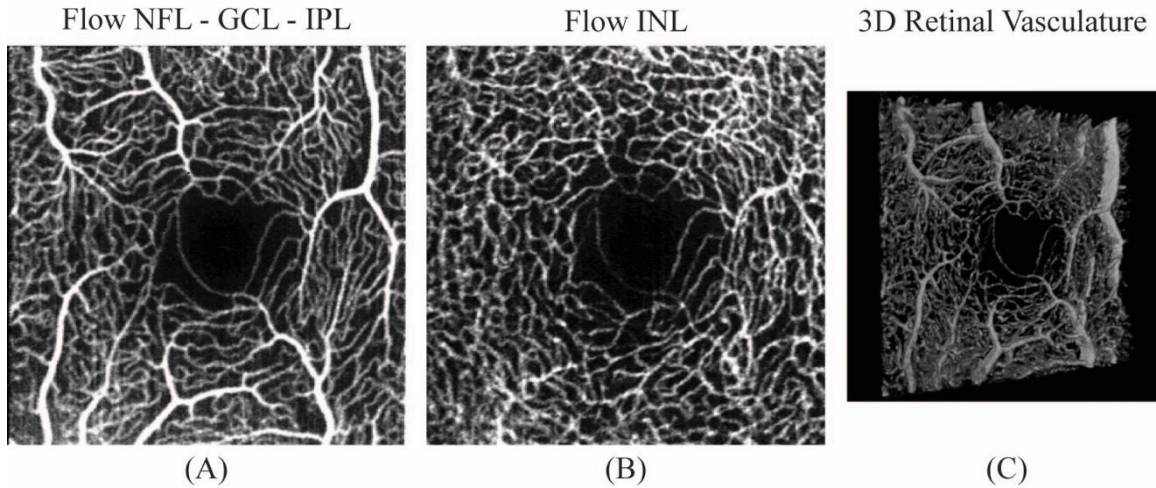


Figure 5.14: High-quality artifact-free angiograms of the retina by compounding eight data sets from the same location with a surface area of $2.0 \times 2.0 \text{ mm}^2$. The yellow scale-bars are $250 \mu\text{m}$ in length. (A) Angiogram of the NFL-GCL-IPL layer clearly showing the vasculature around the foveal avascular zone. (B) Angiogram of the INL-OPL layer showing a fine vascular network. (C) Three-dimensional rendering of the entire retinal vasculature to visualize its orientation in depth (Courtesy of Braaf et al. 2013).

5.7 Summary

The TSLO-AOSLO hybrid system provides both optical and digital eye-tracking capabilities to track the retina over a larger range of motion than previously possible in our AOSLO system alone. The TSLO enables a larger FOV to orient the operator and more easily locate retinal landmarks. High-resolution eye-tracking, with an accuracy of down to a single cone photoreceptor, was shown.

The TSLO-OCT hybrid system was able to perform high fidelity volume scans and generate artifact-free structural images and angiograms of the retina. With the use of a custom validity signal, the TSLO system was able to actively communicate with the OCT and alert the system to remove corrupted B-scans and re-scan affected areas.

5.8 Conclusion

The TSLO system is capable of providing external eye-tracking for high-resolution imaging systems such as AOSLO and OCT. By actively feeding the motion traces of the TSLO into an external active mirror, the TSLO was able to actively steer an imaging beam to stay on target. In the future, this could allow for more robust imaging and functional testing of normal subjects and patients with fixational instability.

5.9 Acknowledgements

The efforts of this Chapter for sections 5.3.2-5.5 were published as a first-author manuscript in *Biomedical Optics Express* in July of 2015. Section 5.6.1 showcased figures that were published as co-author manuscripts in *Biomedical Optics Express* in December of 2012 and January of 2013. Some of the research was performed at the Rotterdam Ophthalmic Institute with assistance from Kari Vienola, Boy Braaf and Koenraad Vermeer. This research was supported by grants from the Macula Vision Research Foundation (AR, CKS), the National Institutes of Health EY014735 (AR, DWA, QY), T32EY007043 (CKS), Stichting Wetenschappelijk Onderzoek Oogziekenhuis Prof. Dr. H.J. Flieringa (SWOO), the Combined Ophthalmic Research Rotterdam (CORR), and Fight for Sight (RS). Ramkumar Sabesan holds a Career Award at the Scientific Interface from the Burroughs Wellcome Fund. Scott Stevenson and Girish Kumar provided the offline motion analysis software.

Dissertation Summary

The primary aims of the studies outlined in this document were to: (1) design, build, and characterize a tracking SLO to provide high quality retinal images and targeted stimulus delivery, (2) modify the TSLO system to perform functional testing using incremental stimuli on patients with focal retinal lesions, and (3) integrate the TSLO and AOSLO systems to demonstrate external active eye-tracking capabilities.

The TSLO system was successfully designed to be a diffraction-limited system. We used an out of plane design, with the tilting of curved mirrors in both the x and y directions, to compensate for system astigmatism and limit overall aberrations (Gomez-Vieyra et al., 2009). The system was built with a flexible field of view, as well as the ability to use varying pupil sizes (2-4 mm) for imaging. Additionally, we showed that the same image-based eye-tracking techniques used in the AOSLO for targeted stimulus delivery could be implemented into a more traditional, larger field of view, confocal SLO system. Eye-tracking with the TSLO was achieved at an accuracy of 0.20 arcminutes and the stimulus stabilization accuracy was found to be 0.66 arcminutes (without TCA).

Next, the TSLO system was modified to perform functional testing using incremental stimuli on patients with focal retinal lesions. With the addition of a stimulus delivery arm ($\lambda = 532$ nm), we were able to perform functional testing on one patient with diagnosed toxoplasmosis scarring and one patient with a subclinical unknown retinal pathology. Using a 40-trial QUEST staircase (with a yes/no response paradigm), we observed clear differences in the sensitivity between areas of complete vision loss and areas adjacent to these lesions in a toxoplasmosis patient. Further testing is needed to fully understand the patchy sensitivity areas that this patient exhibits temporal to his scarring.

Finally, the TSLO system was integrated with the AOSLO system. Eye motion signals were extracted from the TSLO and fed into the AOSLO in order to guide the imaging beam. This hybrid system was then able to compensate for eye motion via the combination of both optical and digital tracking with an average amplitude reduction of 95%. System bandwidth fell slightly short of the computed bandwidth: 84% at 10 Hz, with a 50% correction cutoff of just over 30 Hz. This drop in overall performance was due to the fact that the active tracking mirror had to both drive a sawtooth signal as well as track the eye. Overall, motion that would have been originally too large to track with the AOSLO beam alone was now accounted for using the TSLO-AOSLO hybrid system.

In conclusion, the TSLO system can perform as a stand-alone eye-tracking system or provide active eye-tracking for other high-resolution imaging systems. Additionally, it has the capability to deliver stimuli (in both decrement and increment fashion) to targeted retinal locations.

REFERENCES

- ANSI. (2014). American National Standard for the Safe Use of Lasers ANSI Z136.1-2014. Orlando: Laser Institute of America).
- Arathorn, D.W., Yang, Q., Vogel, C.R., Zhang, Y., Tiruveedhula, P., Roorda, A. "Retinally stabilized cone-targeted stimulus delivery." *Optics Express* 15(21), 13731-13744 (2007).
- Braaf, B., Vienola, K.V., Sheehy, C.K., Yang, Q., Vermeer, K.A., Tiruveedhula, P., Arathorn, D.W., Roorda, A., and de Boer, J.F. "Real-time eye motion correction in phase-resolved OCT angiography with tracking SLO." *Biomedical Optics Express* 4(1); 51-65 (2013).
- Burns, S.A., Tumber, R., Elsner, A.E., Ferguson, D., and Hammer, D.X. "Large-field-of-view, modular, stabilized, adaptive-optics-based scanning laser ophthalmoscope." *Journal of the Optical Society of America A* 24(5), 1313-1326. (2007).
- Burr, D.C., and Ross, J. "Contrast sensitivity at high velocities." *Vision research* 22(4): 479-484, (1982).
- Cherici, C., Kuang, X., Poletti, M., & Rucci, M. "Precision of sustained fixation in trained and untrained observers." *Journal of Vision* 12(6): 31, 1-16 (2012).
- Choe, K.W., Blake, R., and Lee, S-H. "Pupil size dynamics during fixation impact the accuracy and precision of video-based gaze estimation." *Vision research*, <http://www.sciencedirect.com/science/article/pii/S0042698915000024>, doi:10.1016/j.visres.2014.12.018, (2015).
- Clarke, F.J.J., Belcher, S.J. "On the localization of Troxler's effect in the visual pathway." *Vision Research* 2; 53-68 (1962).
- Collewijn, H., van der Mark, F., Jansen, T.C. "Precise recording of human eye movements." *Vision Research* 15; 447-455, (1975). doi: 10.1016/0042-6989(75)90098-X.
- Coppola D., Purves D. "The extraordinarily rapid disappearance of entopic images." *Proc Natl Acad Sci USA*, 93, 8001-4 (1996).
- Cornsweet, T.N. "New technique for the measurement of small eye movements." *JOSA* 48, 808-811 (1958).
- Cornsweet, T. N. and Crane, H. D. "Accurate two-dimensional eye tracker using first and fourth Purkinje images," *J. Opt. Soc. Am.* 63(8), 921-928 (1973).
- Crane, H. D., and Steele, C. M. "Generation-V dual-Purkinje-image eye tracker," *Appl. Opt.* 24(4), 527-537 (1985).

Curcio, C.A., Sloan, K.R., Kalina, R.E. and Hendrickson, A.E. "Human photoreceptor topography." *Journal of Comparative Neurology*, 292(4), 497-523 (1990).

Donnelly III, W.J., Roorda, A. "The Optimal Pupil Size in the Eye for Axial Resolution" *J. Opt. Soc Am. A*. 20(11): 2010-2015 (2003).

Drewes, J., Masson, G. S., & Montagnini, A. "Shifts in reported gaze position due to changes in pupil size: Ground truth and compensation." *Proceedings of the symposium on eye tracking research and applications*, ACM, 2012.

Drewes, J., Zhu, W., Hu, Y., & Hu, X. "Smaller Is Better: Drift in Gaze Measurements due to Pupil Dynamics." *PLOS*, <http://journals.plos.org/plosone/article?id=10.1371/journal.pone.0111197>, DOI: 10.1371/journal.pone.0111197 (2014).

Dubra, A. & Sulai, Y. "Reflective afocal broadband adaptive optics scanning ophthalmoscope." *Biomedical Optics Express* 2, 1757-68 (2011).

Dubra, A., Sulai, Y.N., Norris, J.L., Cooper, R.F., Dubis, A.M., Williams, D.R., Carroll, J. "Noninvasive imaging of the human rod photoreceptor mosaic using a confocal adaptive optics scanning ophthalmoscope." *Biomedical Optics Express* 2(7), 1864-1876 (2011).

Engbert, R. & Kliegl R. "In The Mind's Eyes: Cognitive and Applied Aspects of Eye Movements." Elsevier, Oxford, 103–117, (2003).

Enoch, J.M., Le, D.A. "Comparison of the Canon CPP-1 and the new Nidek MP-1 45 degree fundus camera perimeters: studies around and on top of the optic nerve head in myopia." *Invest Ophthalmol Vis Sci*; 45:E-Abstract 2772 (2004).

Ferguson, R.D., Hammer, D.X., Paunescu, L.A., Beaton, S., and Schuman, J.S. "Tracking optical coherence tomography." *Optics Letters* 29(18), 2139-2141 (2004).

Ferguson, R.D., Zhong, Z., Hammer, D.X., Mujat, M., Patel, A.H., Deng, C., Zou, W., & Burns, S.A. "Adaptive optics scanning laser ophthalmoscope with integrated wide-field retinal imaging and tracking." *Journal of the Optical Society of America*, A27(11), A265-A277 (2010).

Findlay, J. M. "Frequency analysis of human involuntary eye movement." *Kybernetik*, 8(6), 207-214, (1971).

Garcia-Martin, E., Pinilla, I., Sancho, E., Almarcegui, C., Dolz, I., Rodrigues-Mena, D., Fuertes, I., Cuenca, N. "Optical Coherence Tomography in Retinitis Pigmentosa: Reproducibility and Capacity to Detect Macular and Retinal Nerve Fiber Layer Thickness Alterations." *Retina* 32, 8: 1581-1591 (2012).

Gómez-Vieyra, A. Dubra, D. Malacara-Hernández & D.R. Williams. "First-order design of off-axis reflective ophthalmic adaptive optics systems using afocal telescopes." *Optics Express* 17, 18906-19 (2009).

Guizar-Sicairos, M., Thurman, S.T. & Fienup, J.R." Efficient subpixel image registration algorithms." *Optics letters* 33, 156-8 (2008).

Hafed Z., Clark J. "Microsaccades as an overt measure of covert attention shifts." *Vision Research*, 42:2533–2545 (2002).

Hammer, D. X., Ferguson, R. D., Magill, J. C., White, M. A., Elsner, A. E., & Webb, R. H. (2003, July). "Tracking scanning laser ophthalmoscope (TSLO)." *Biomedical Optics*, 208-217, International Society for Optics and Photonics (2003).

Hammer, D.X., Ferguson, R.D., Iftimia, N.V., Ustun, T., Wollstein, G., Ishikawa, H., Gabriele, M.L., Dilworth, W.D., Kagemann, L, Schuman, J.S. "Advanced scanning methods with tracking optical coherence tomography." *Optics Express* 13(20), 7937-7947 (2005).

Hammer, D.X., Ferguson, R.D., Bigelow, C.E., Iftimia, N.V, Ustun, T.E. & Burns, S.A. "Adaptive optics scanning laser ophthalmoscope for stabilized retinal imaging." *Optics Express* 14(8), 3354-3367 (2006).

Harmening, W.M., Tiruveedhula, P., Roorda, A., Sincich, L.C. "Measurement and correction of transverse chromatic offsets for multi-wavelength retinal microscopy in the living eye." *Biomedical Optics Express* 3(9), 2066-2077 (2012).

Harmening, W.H., Tuten, W.S., Roorda, A., Sincich, L.C.. "Mapping the Perceptual Grain of the Human Retina." *The Journal of Neuroscience* 34(16), 5667-5677 (2014).

Helmholtz, H. "Physiological optics." Trans, from Third German Edition., J. P. C. Southall (Ed.). Menasha, Wisconsin: G, Banta Co., 1924-25. Vol. II, p. 266.

Jurin, J. "An essay on distinct and indistinct vision." In: Smith R. (ed.) *A complete system of opticks in four books*, Cambridge: Published by the author, pp. 115–171 (1738).

Kimmel, D.L., Mammo, D. and Newsome, W.T. "Tracking the eye non-invasively: simultaneous comparison of the scleral search coil and optical tracking techniques in the macaque monkey." *Frontiers in behavioral neuroscience*, 6 (2012).

Ko, H.-K., Poletti, M., and Rucci, M. "Microsaccades precisely relocate gaze in a high visual acuity task." *Nature Neuroscience*, 13, 1549–1553 (2010).

Kocaoglu, O.P., Ferguson, R.D., Jonnal, R.S., Liu, Z., Wang, Q., Hammer, D.X., & Miller, D.T. "Adaptive optics optical coherence tomography with dynamic retinal tracking." *Biomedical Optics Express* 5(7), 2262-2284 (2014).

Kowler, E., and Steinman, R.M. "Miniature saccades: eye movements that do not count." *Vision Res.* 19, 105–108 (1979).

Kowler, E., and Steinman, R.M. "Small saccades serve no useful purpose: reply to a letter by R.W. Ditchburn." *Vision Res.* 20, 273– 276 (1980).

Kumar, G., and Chung, S.T. "Characteristics of Fixational Eye Movements in People with Macular Disease." *Investigative Ophthalmology & Visual Science* 55(8), 5125-5133 (2014).

Lakshminarayanan V., Knowles R.A., Enoch J.M., & Vasuvedan R. "Measurement of fixational stability while performing a hyperacuity task using the scanning laser ophthalmoscope: preliminary studies." *Clinical Vision Sciences* 7, 557-563 (1992).

Leigh, R.J. and Zee, D.S. "The Neurology of Eye Movements." Oxford University Press, Oxford (2006).

Liang, J., Williams, D.R., Miller, D.T. "Supernormal vision and high-resolution retinal imaging through adaptive optics." *Journal of the Optical Society of America A* 14(11), 2884-2892 (1997).

Martinez-Conde, S., Macknik, S. L., & Hubel, D. H. "The role of fixational eye movements in visual perception." *Nature Reviews Neuroscience*, 5(3), 229-240 (2004).

Martinez-Conde, S., Macknik, S. L., Troncoso, X. G., & Dyar, T. A. "Microsaccades counteract visual fading during fixation." *Neuron*, 49(2), 297-305 (2006).

Martinez-Conde, S. "Fixational eye movements in normal and pathological vision." *Progress in brain research*, 154, 151-76 (2006).

Martinez-Conde, S., Macknik, S. L., Troncoso, X. G., & Hubel, D.H. "Microsaccades: a neurophysiological analysis." *Trends in Neurosciences* 32, 463-75 (2009).

McCamy, M.B., Otero-Millan, J., Leigh, R.J., King, S.A., Schneider, R.M., Macknik, S.L. and Martinez-Conde, S. "Simultaneous Recordings of Human Microsaccades and Drifts with a Contemporary Video Eye Tracker and the Search Coil Technique." *PloS one*, 10(6) (2015).

Merino, D., Duncan, J.L., Tiruveedhula, P., Roorda, A. "Observation of cone and rod photoreceptors in normal subjects and patients using a new generation adaptive optics scanning laser ophthalmoscope." *Biomedical Optics Express* 2, 2189-201 (2011).

Midena, E. "Liquid Crystal Display Microperimetry in Perimetry and the Fundus: An Introduction to Microperimetry." Slack Inc., Thorofare, pp. 15–26 (2007).

Mulligan, J.B. "Recovery of motion parameters from distortions in scanned images," in Proceedings of the NASA Image Registration Workshop (IRW97) (NASA Goddard Space Flight Center, MD, 1997).

Nachmias, J. "Determiners of the drift of the eye during monocular fixation." *JOSA*, 51(7), 761-766 (1961).

Ott, D. & Eckmiller, R. "Ocular torsion measured by TV- and scanning laser ophthalmoscopy during horizontal pursuit in humans and monkeys." *IOVS* 30, 2512-2520 (1989).

Ott, D. & Daunicht, W.J. "Eye movement measurement with the scanning laser ophthalmoscope." *Clin. Vision Sci.* 7, 551-556 (1992).

Poonja, S. Patel, S., Henry, L. & Roorda, A. "Dynamic visual stimulus presentation in an adaptive optics scanning laser ophthalmoscope." *Journal of refractive surgery* 21, S575-80 (2005).

Porter, J., Queener, H., Lin, J., Thorn, K., Awwal, A.A. "Adaptive optics for vision science: Principles, practices, design and applications." (John Wiley & Sons, 2006), Chap. 10.

Ratliff, F., & Riggs, L. A. "Involuntary motions of the eye during monocular fixation." *Journal of experimental psychology*, 40(6), 687 (1950).

Riggs, L. A., Armington, J.C., and Ratliff, F. "Motions of the retinal image during fixation," *J. Opt. Soc. Am.* 44(4), 315–321 (1954).

Riggs, L. A., and Schick, A. M. "Accuracy of retinal image stabilization achieved with a plane mirror on a tightly fitting contact lens." *Vision Res.* 8(2), 159–169 (1968).

Robinson, D.A. "A method of measuring eye movements using a scleral coil in a magnetic field." *IEEE Trans Biomed Eng.*, 10, 137–145, (1963). doi: 10.1109/tbmel.1963.4322822

Rolfs, M. "Microsaccades: small steps on a long way." *Vision research* 49, 2415-41 (2009).

Roorda, A., Romero-Borja, F., Donnelly III, W., Queener, H., Hebert, T., & Campbell, M. "Adaptive optics scanning laser ophthalmoscopy." *Optics Express*, 10(9), 405-412 (2002).

Rucci, M., Iovin, R., Poletti, M., and Santini, F. "Miniature Eye Movements Enhance Fine Spatial Detail." *Nature*. 447(7146), 851-854 (2007).

Sadda, S.R., Keane, P.A., Ouyang, Y., Updike, J.F. & Walsh, A.C. "Impact of scanning density on measurements from spectral domain optical coherence tomography." *Investigative ophthalmology & visual science* 51, 1071-8 (2010).

Santini, F., Redner, G., Iovin, R., and Rucci, M. "EyeRIS: a general-purpose system for eye-movement-contingent display control," *Behav. Res. Methods* 39(3), 350–364 (2007).

Scholtes, A. M. W., & Bouman, M. A. "Psychophysical experiments on spatial summation at threshold level of the human peripheral retina." *Vision Research*, 17(7), 867-873 (1977).

Schuchard, R.A. & Raasch, T.W. "Retinal locus for fixation: pericentral fixation targets." *Clin. Vision Sci.* 7, 511-520 (1992).

Sheehy, C.K., Yang, Q., Arathorn, D.W., Tiruveedhula, P., de Boer, J.F. and Roorda, A. "High-speed, image based eye tracking with a scanning laser ophthalmoscope." *Biomedical Optics Express* 3(10), 2611-2622 (2012).

Simonet, P. and Campbell, M.C. "The optical transverse chromatic aberration on the fovea of the human eye," *Vision Res.* 30 (2), 187–206 (1990).

Sincich, L.C., Zhang, Y., Tiruveedhula, P., Horton, J.C., Roorda, A. "Resolving single cone inputs to visual receptive fields." *Nature Neuroscience* 12(8), 967-969 (2009).

Steinman, R.M., Haddad, G.M., Skavenski, A.A., Wyman, D. "Miniature eye movement." *Science*, 181:810–819 (1973).

Stetter, M., Sendtner, R.A., Timberlake, G.T. "A novel method for measuring saccade profiles using the scanning laser ophthalmoscope." *Vision Res* 36 (13): 1987-94, (1996).

Stevenson, S.B. & Roorda, A. "Correcting for miniature eye movements in high resolution scanning laser ophthalmoscopy." *Proceedings of SPIE* 5688, 145-151 (2005).

Stevenson, S.B., Roorda, A., & Kumar, G. "Eye Tracking with the Adaptive Optics Scanning Laser Ophthalmoscope." *Proceedings of the 2010 Symposium on Eye-Tracking Research and Applications*, Austin, TX, March 22-24, 2010 (ACM, NY) pp: 495-498.

Thibos, L.N., Bradley, A., Still, D.L., Zhang, X., and Howarth, P.A. "Theory and measurement of ocular chromatic aberration," *Vision Res.* 30 (1), 33–49 (1990.)

Tuten, W.S., Tiruveedhula, P., Roorda, A. "Adaptive optics scanning laser ophthalmoscope-based microperimetry." *Optometry and Vision Science* 89(5), 563-574 (2012).

Vienola, K.V., Braaf, B., Sheehy, C.K., Yang, Q., Tiruveedhula, P., Arathorn, D.W., de Boer, J.F. and Roorda, A. "Real-time eye motion compensation for OCT imaging with tracking SLO." *Biomedical Optics Express* 3(11), 2950-2963 (2012).

Vogel, C.R., Arathorn, D.W., Roorda A., & Parker, A. "Retinal motion estimation in adaptive optics scanning laser ophthalmoscopy." *Optics Express* 14, 487-97 (2006).

Wang, Q., Tuten, W.S., Lujan, B.J., Holland, J., Bernstein, P.S., Schwartz, S.D., Duncan, J.L., & Roorda, A. "Adaptive Optics Microperimetry and OCT Images Show Preserved Function and Recovery of Cone Visibility in Macular Telangiectasia Type 2 Retinal Lesions." *Invest Ophthalmol Vis Sci*, 56 (2), 778-786. (2015).

Watson, A. B. and Pelli, D. G. "QUEST: a Bayesian adaptive psychometric method." *Perception & psychophysics*, 33 (2), 113-20 (1983).

Williams, D.R. "Imaging single cells in the living retina." *Vision Research* 51(13), 1379-1396 (2011).

Winter, S., Sabesan, R., Tiruveedhula, P. N., Privitera, C., Lundstrom, L., & Roorda, A. "Objective measurements of transverse chromatic aberration across the visual field of the human eye." *Investigative Ophthalmol Vis Sci* 2015; 56(7):E-Abstract 1730.

Winterson, B.J., and Collewijn, H. "Microsaccades during finely guided visuomotor tasks." *Vision Res.* 16, 1387–1390 (1976).

Woods, R.L., Vera-Diaz, F.A., Lichtenstein, L., Peli, E. "Spatial alignment of microperimeters." *Invest Ophthalmol Vis Sci* 2007; 48:E-Abstract 144.

Yang, Q., Arathorn, D.W., Tiruveedhula, P., Vogel, C.R., & Roorda, A. "Design of an integrated hardware interface for AOSLO image capture and cone-targeted stimulus delivery." *Optics Express* 18(17), 17841-17858 (2010).

Yang, Q., Zhang, J., Nozato, K., Saito, K., Williams, D.R., Roorda, A. & Rossi, E.A. "Closed-loop optical stabilization and digital image registration in adaptive optics scanning light ophthalmoscopy." *Biomedical Optics Express*, 5(9), 3174-3191 (2014).